STUDY OF LOSSES IN HIGH FREQUENCY TRANSFORMERS

A Dissertation
Presented to
The Academic Faculty

By

Xiwei Zheng

In Partial Fulfillment
of the Requirements for the Degree
Master of Science in the
School of Electrical and Computer Engineering

Georgia Institute of Technology

December 2019

STUDY OF LOSSES IN HIGH FREQUENCY TRANSFORMERS

Approved by:

Dr. Deepakraj M. Divan, Advisor
School of Electrical and Computer Engineering
Georgia Institute of Technology

Dr. J. Rhett Mayor, Advisor
School of Mechanical Engineering
Georgia Institute of Technology

Dr. Maryam Saeedifard
School of Electrical and Computer Engineering
Georgia Institute of Technology

Dr. Lukas Graber
School of Electrical and Computer Engineering
Georgia Institute of Technology

Date Approved: August 23, 2019

Dedicated to my beloved parents

ACKNOWLEDGEMENTS

First and the formost, I would first like to express my deepest appreciation to my thesis advisor Dr. Deepak Divan and co-advisor Dr. Rhett Mayor for their support and guidance during my master study. Without their encouragement, inspiration, motivation, and immense knowledge, this could not been possible. The enthusiasm, confidence, patience and steadiness I learned from them will always help me to overcome the obstacles in the future.

Further, I would like to thank my committee members Dr. Maryam Saeedifard and Dr. Lukas Graber, for their advice, guidance, and encouragement.

In addition, I would like to thank the Center for Distributed Energy. It has been a great journey working and learning with everyone at CDE. Without their help and encouragement, I would not accomplish this. I would like to thank Yunkyung Chang-Hoffman and Brandon Royal, for their logistic support and mechanical support, so that I could finish the projects quickly and nicely. In particular, I would express my deep appreciation to Prasad Kandula for guiding me during my research. I also would like to personally thank Mickael Mauger, Xiangyu Han, Zheng An, and Liran Zheng for your support and mentor-ship. This accomplishment would not have been possible without all of you at CDE.

Finally, I would like to express my profound gratitude to my parents for their continuous support and encouragement thought out the years. Also thanks to my host parents Brad and Katy for their support and guidance.

TABLE OF CONTENTS

Acknowledgments iv

List of Tables vii

List of Figures viii

Chapter 1: Introduction 1

1.1 Background 1

1.2 Research Objective 3

Chapter 2: High Frequency Transformer 5

2.1 Introduction 5

2.2 Transformer Design 5

2.2.1 Permanent Magnets 8

2.3 Transformer Parametric Circuit Model 10

2.4 Magnetic Circuit Model 13

2.5 Transformer Characterization 15

2.6 Conclusion 18

Chapter 3: Copper Loss 23

3.1 Introduction 23

3.2 Winding Copper Loss Calculation in Active and Open Winding During Energy Transfer States . . . 23

3.2.1 AC Current Distribution in S4T windings . . . 23

3.2.2 AC Resistance Factor and Loss Calculation of Active Winding . . . 25

3.2.3 AC Resistance Factor and Loss Calculation of Open Winding . . . 25

3.3 Verification of Loss in Open winding using FEM analysis . . . 28

3.4 Winding Copper loss calculation during transition states . . . 31

3.5 Experimental Tests . . . 34

3.6 Loss estimation for a 25 kVA 480/480 V S4T . . . 37

3.7 Conclusion . . . 42

Chapter 4: Core loss . . . 43

4.1 Introduction . . . 43

4.2 Test setup . . . 44

4.3 Core Loss without DC Bias . . . 46

4.4 Core Loss with DC Bias . . . 49

4.5 Discussion . . . 50

Chapter 5: Conclusion . . . 53

5.1 Future Work . . . 54

References . . . 58

LIST OF TABLES

2.1 Transformer design specifications 7

2.2 Permanent magnets specifications 10

3.1 Specification of HF transformer. 40

4.1 Core specifications 44

4.2 Measured core losses without DC bias for different ΔB 47

LIST OF FIGURES

1.1 Topology for the three-phase soft-switching solid state transformer (S4T) . 2

1.2 Operation of Soft-Switching Solid-State Transformer (S4T). 4

2.1 Prototype high-frequency transformer with permanent magnets. 5

2.2 Multi-objective S4T transformer design. 7

2.3 Transformer design with permanent magnets to offset DC bias 8

2.4 Usable B-H curve range. 9

2.5 Equivalent Circuit of the transformer with isolation 11

2.6 Interleaved foil winding transformer 12

2.7 Equivalent magnetic circuit for the transformer design with permanent magnets 14

2.8 Transformer design with permanent magnets to offset DC bias 15

2.9 Finite element analysis simulation of two transformer designs at 60A excitation 16

2.10 Double Pulse Test (DPT) Setup 17

2.11 Theoretical gate signal voltage and current waveform 18

2.12 DPT Test Circuit Operating Principles 19

2.13 DPT results of foil winding transformer without magnets. 20

2.14 DPT results of foil winding transformer with magnets. 21

3.1 AC current distribution. 24

3.2 Current distribution in active winding and open winding at different Δ. . . . 26

3.3 AC resistance factor 27

3.4 Model used to evaluate eddy current distribution and losses in open winding of S4T transformer in ANSYS Maxwell. 29

3.5 The magnetic field (H) measured along the axis, redline shown in Figure 3.4. 29

3.6 Current density plots across the windings for 3kHz and 10kHz. 30

3.7 Current density magnitude and phase distribution measured along the axis in Figure 3.4 32

3.8 AC resistance factor 33

3.9 Primary and secondary current during transition state. 34

3.10 AC copper loss measurement test setup. 35

3.11 AC resistance factor 36

3.12 Experimental result of AC resistance factor 38

3.13 Multi-objective S4T transformer design. 39

3.14 Loss estimation for 25 kVA 480 V/480 V S4T transformer at different frequencies. 41

4.1 C-core dimension standard 44

4.2 Test setup 45

4.3 Test waveform for ΔB_{pp}=250 mT at B_{DC}=0 T 47

4.4 Measured core losses compare to Steinmetz and iGSE for different ΔB_{pkpk} at no DC bias 48

4.5 Test waveform for ΔB_{pp}=250 mT at B_{DC}=0.8T 50

4.6 Under DC bias condition for different ΔB_{pkpk} 51

SUMMARY

The Soft-Switching Solid-State Transformer (S4T) is promised to be the next generation converter that has flexible inputs and outputs, galvanic isolation, bi-directional power flow capability, soft switching over the entire load range, controlled dv/dt, and benign failure modes.

The high-frequency transformer is a key component in solid state transformer. Transformer is design to be low cost, low loss, low leakage inductance, low inter-winding capacitance and small volume. In the S4T, the high-frequency transformer is similar to a fly-back transformer. The high-frequency transformer is acting as an energy transfer link between the input and output. It is important to understand the losses in the high-frequency transformer and address the losses with appropriate thermal management.

The operation cycle of the transformer in S4T is unique. Only one winding is active during the active energy transfer time, and additional transition stages to ensure soft switching. There is significant proximity effect which induced eddy current losses in the inactive winding. The transition stages result in some unique AC copper loss in the winding as well. Because the magnetizing current is mainly DC with an AC ripple, the high-frequency transformer also has a unique feature of DC biased flux. Permanent magnets are used to pre-bias the core so that usable B-H curve range can be extended. The non-sinusoidal magnetizing current and the usage of permanent magnets result in different losses. DC bias are known to significantly affect core loss and whether permanent magnets can offset the DC bias and neutralize the loss in the core needs careful examination.

The dissertation identify all the loss components in the high-frequency transformer and presents analysis to evaluate these losses. Numerical method to estimate the losses are proposed. FEM analysis to verify the analytical method is presented. These results are compared with experimental results.

CHAPTER 1
INTRODUCTION

1.1 Background

Transformer is a passive electrical device that transfers electrical energy from input to output, and has a basic structure of two or more windings placed around a common magnetic core. Transformers have become essential for the transmission, distribution, and utilization of alternating current electric power. Throughout the years of development, transformers are mature products, which are very rugged, inexpensive and reliable. Even though the typical power transformer is well developed and designed to provide isolation between the windings, there are several drawbacks. The transformer is bulky, operate at 60 Hz, and completely passive, so it is not possible to improve performance.

The idea of using power electronics and high frequency isolation to directly interface with the grid has attracted tremendous attention. The Solid State Transformer (SST), as a replacement for the 60 Hz transformer, converts available medium voltage to desired low voltage AC or DC [1]. The ability to provide high frequency galvanic isolation offers reduction in size. The high-frequency transformer is the key element of SST since it act as an energy transfer element. Soft-Switching Solid-State Transformer (S4T) is an implementation of SST. S4T promises to be a next generation converter that has flexible inputs and outputs, galvanic isolation, bi-directional power flow capability, full range soft switching, controlled dv/dt and benign failure modes. Figure 1.1 shows the topology for three phase S4T.

Unlike the traditional transformers which is passive and operate at 60 Hz, S4T is bidirectional power electronic converter switching around 20 kHz. The design of the high-frequency transformer has an important influence on overall system weight, power con-

version efficiency, and cost. Therefore high-frequency transformer need to meet the design requirements of small size, low losses, relative low cost, low leakage inductance, and low inter-winding capacitance. However these parameters are interdependent and trade-offs becomes necessary to achieve the optimal design. It is important to characterize the high-frequency transformer parasitic elements and analysis the loss components due to the unique operation cycles.

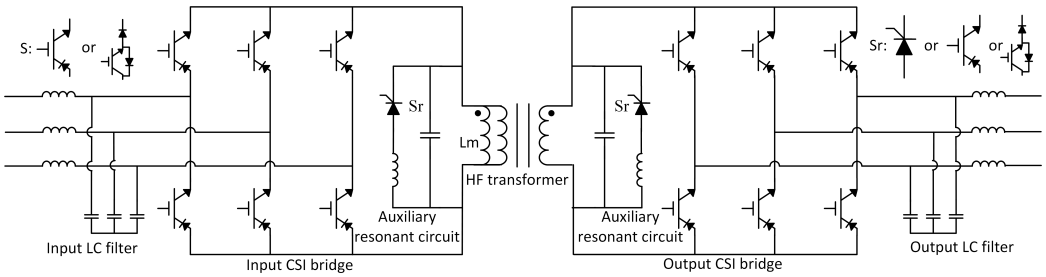

Figure 1.1: Topology for the three-phase soft-switching solid state transformer (S4T)

With the increase in switching frequency, new design challenges arise and development that is required of the magnetic components. There are the main concern with the increase in losses as well as the desire to minimize volume and footprint. Parasitic elements of magnetic components would affect the converter operation more and more as the frequency gets higher and higher. Operating at a higher frequency has many benefits, the first of which is size. For any given power rating, the higher the frequency, the smaller the transformer can be. Second, because the transformer is smaller, less copper wire is needed, thus reducing the copper loss and helping to make the transformer more efficient. Also, there are magnetic core material specific design for high frequency operation and can be used to replace ferrite cores. However, the benefits brought about by light weight, small size, and higher power density, pose a number of challenges. Minimizing the issues such as skin and proximity effects are a serious concern when analyzing the copper losses in high-frequency transformers. Also using new magnetic material such as nanocrystalline for transformer cores needs to be characterized to fully understand the core loss under S4T operation condition. Therefore, this work focus on identify loss components involved in

the high-frequency transformer so that proper thermal management can be proposed.

1.2 Research Objective

High-frequency transformer is an important component in any solid state transformer, since it is a energy transfer link between the input and output. Its operation principle is similar to a flyback DC/DC converter, where the magnetizing inductance of the transformer is used to temperately store energy. Figure 1.2 shows the operation of the high-frequency transformer in S4T. The operation cycle start with one of the bridges charging the transformer from the input source and ends with the other bridge discharging the transformer into the output. These two active states are interspersed with transition states, controlled using the resonant circuits, to ensure soft switching. Unlike most SST, which the transformer leakage inductance acts as an energy transfer element. For S4T, it is the transformer magnetizing inductance. So the transformer leakage inductance need to be kept low while maintaining the desired insulation level. Another issue is winding-to-winding capacitance need to be kept low, because it causes common mode current flow when devices are switched at a high dv/dt rate [2].

Apart from low cost and low loss design requirements for transformer, there are new challenges such as low leakage inductance, low winding-to-winding capacitance and minimize core volume [2]. After understanding the design constrains, two transformer winding designs are proposed, which are copper foil winding and coaxial litz wire winding. Since the transformer is operating at 16kHz, it is important to understand the winding loss [3]. The winding loss consist of dc winding loss and ac winding loss. DC winding loss simply depends on winding resistance and current. AC winding loss plays a big role and is consist of active winding loss, open winding loss, resulting from skin effect and proximity effect, and transition loss. Mathematical derivations to calculate these unique AC loss are proposed. FEM analysis to verify the analytical methods is presented. Experimental results of measuring copper foil AC loss are presented for verification.

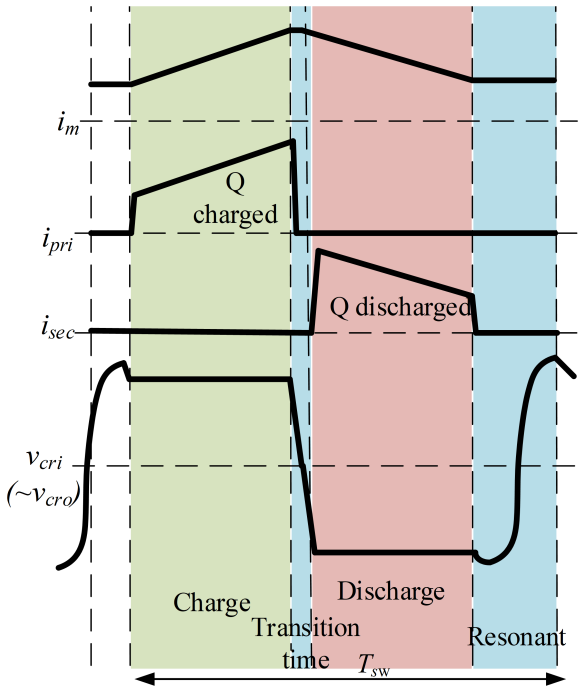

Figure 1.2: Operation of Soft-Switching Solid-State Transformer (S4T).

The high-frequency of the S4T has an unique feature of DC biased flux. As shown in Figure 1.2, the total magnetizing current is primarily DC with AC ripple. That DC current create a DC bias flux in the core and restricted the peak operation flux density in the core. Since transformer size is determined by the maximum flux density of the magnetic core, permanent magnets are introduced to provide a pre-biased flux for the magnetic core. Therefore the usable B-H curve range is extended to save magnetic material. With such a complex and unique high-frequency design, Steinmetz equation provided by manufacture can no longer provide an accurate estimation of the core loss. The non-sinusoidal AC current, DC biased in the core and eddy current in the permanent magnets brings complexity when analyzing the core loss[4]. Therefore, it is important and necessary to study the core loss in detail. Experimental results on nanocrystalline magnetic material from MK Magnetics will be presented.

This work will focus on characterize the high-frequency transformer, analysis the AC winding loss and core loss in the unique designed high-frequency transformers. Experimental results along with mathematical derivations and FEM analysis will be presented.

CHAPTER 2

HIGH FREQUENCY TRANSFORMER

2.1 Introduction

The high-frequency transformer is a key element of the Soft-Switching Solid-State Transformer (S4T). It provides energy transfer link between the input and the output with galvanic isolation. This chapter will present the design of high-frequency transformer with permanent magnets, which can provide significant saving on magnetic materials. It is important to understand the parasitic elements of the transformer due to its unique design. ANSYS Maxwell is used to build FEM model of the transformer and verify the design parameters. Experimental results of the prototype transformer characterization will also be presented.

2.2 Transformer Design

The high frequency transformer design need to meet the following requirements: low cost, low volume, low loss, low leakage inductance, and low inter winding capacitance. A

(a) foil winding (b) coaxial litz wire

Figure 2.1: Prototype high-frequency transformer with permanent magnets.

high-frequency transformer design for S4T has been proposed before[2]. Detailed design considerations and transformer operation states are discussed. A summary of the design and transformer operation condition will be provided in this section. The proposed design is for foil winding only and air gap is distribute on both side of the transformer. In this chapter, two transformer designs with permanent magnets for DC flux bias will be proposed. One is interleaved foil winding, one is coaxial litz wire winding. Air gap for both transformer designs are on the non-winding core leg. Both high-frequency transformer design are fabricated and being characterized. Detailed characterization results will be discussed later. Figure 2.1a is a picture of the prototype transformer using interleaved foil winding. Figure 2.1b is a picture of the prototype transformer wound with coaxial litz wire.

Design specifications for a 25 kVA 16 kHz interleaved foil winding transformer for a 3-phase 480 V S4T application is listed in Table 2.1. Winding loss is calculated using proposed analytical method from Chapter 3. Core loss is estimated using improved Generalized Steinmetz equation (iGSE). The Steinmetz equation parameters for the core loss are provided by manufacture [5]. The effect of DC offset is neglected for this analysis. The transformer design is optimized across various parameters such as total loss, leakage inductance, parasitic capacitance, cost, size (core area A_e x window area A_w) for various combinations of turns and magnetizing inductance (L_m).The results of the multi-objective design is shown in a radar plot in Figure 2.2. The design with magnetizing inductance of 400 μH and 14 turns satisfies all objectives optimally. Nanocrystalline soft magnetic material is a fairly new development. The material composition is 82% iron with the remaining balance silicon,boron, niobium, copper, carbon, molybdenum, and nickel. This material is promising to have the best overall performance over a broad range of frequencies when compared to other available materials. It has a relatively high saturation flux density (1.2 T), combined with its incredible low loss and high permeability through a wide frequency range, makes it useful in many applications. So two of SC2061M1 nanocrystalline cores from MK Magnetics are chosen for the design.

Table 2.1: Transformer design specifications

Parameters	**Value**
Switching freq	16 kHz
Loss	$< 0.5\%$
Foil	11 mils thick, $3''$ wide
Insulation	3 mil kapton
Turns ratio	1:1
Magnetizing inductance L_m	200 μH - 400 μH
Leakage inductance L_{lk}	$< 1\%$ of L_m
Winding-to-winding capacitance C_w	<1 nF
Saturation current I_{sat}	140 A

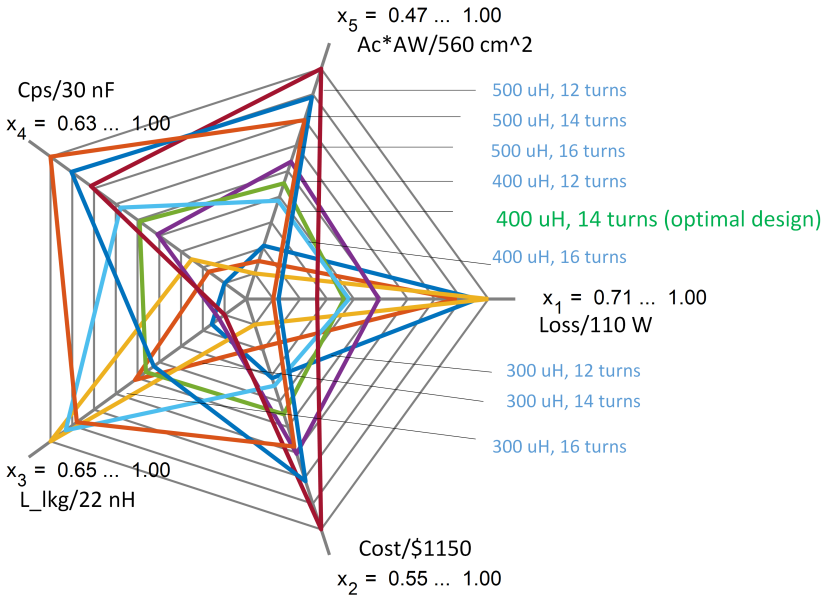

Figure 2.2: Multi-objective S4T transformer design.

The high-frequency transformer with coaxial cable is design with same parameters as listed in Table 2.1, except foil windings are not used [6]. The coaxial cable part number is CW8301 from Cooner wire. The coaxial litz wire is custom made with the PFA insulation between the inner litz wire and outer shield rated for 30 kV. The inner litz wire is 52/33 AWG, which is 16 AWG equivalent. And the outer shield is 16 AWG equivalent using 34 AWG wire. Coaxial cable are wound 15 turns per layer and 6 layers, with each layer connected in parallel. Two of nanocrystalline core SC2062M1 from MK magnetics are used.

2.2.1 Permanent Magnets

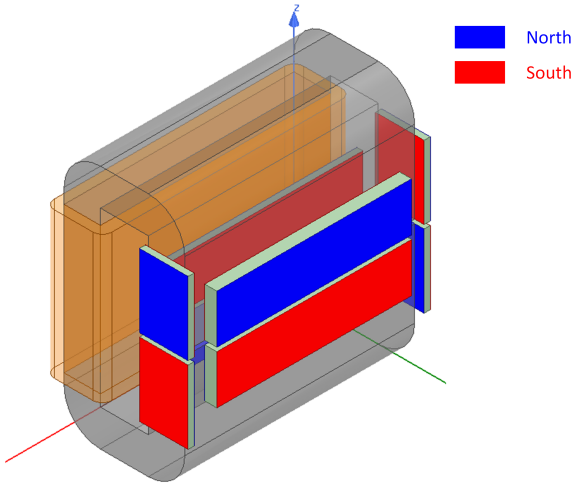

Figure 2.3: Transformer design with permanent magnets to offset DC bias

When designing the S4T high-frequency transformer, the peak flux density through the core should be kept below the saturation point of the B-H curve, as shown in equation (2.1), in which B_w is the flux density due to the winding excitation, and B_{sat} is the saturation flux density of the core. Therefore, the transformer size is determined by the maximum flux density of the magnetic core when the design is driven by saturation flux density. S4T has a unique feature of dc-biased flux in the transformer magnetizing inductance, which means that the working point is restricted within the first quadrant of the B-H curve while the region of the third-quadrant is not utilized.

$$B_w \leq B_{sat} \tag{2.1}$$

Considering this dc-biased flux feature, permanent magnets can be integrated with the magnetic materials to provide a pre-biased flux for the core [7]. The flux generated by the permanent magnets should be in a reverse direction to the flux excited by the windings. As shown in equation (2.2), the resultant equivalent flux density (B_{eq}) within the core will be the flux density of the excitation from the winding (B_w) minus the flux density caused by permanent magnets (B_{pm}). If the core flux density is kept below the saturation level, more

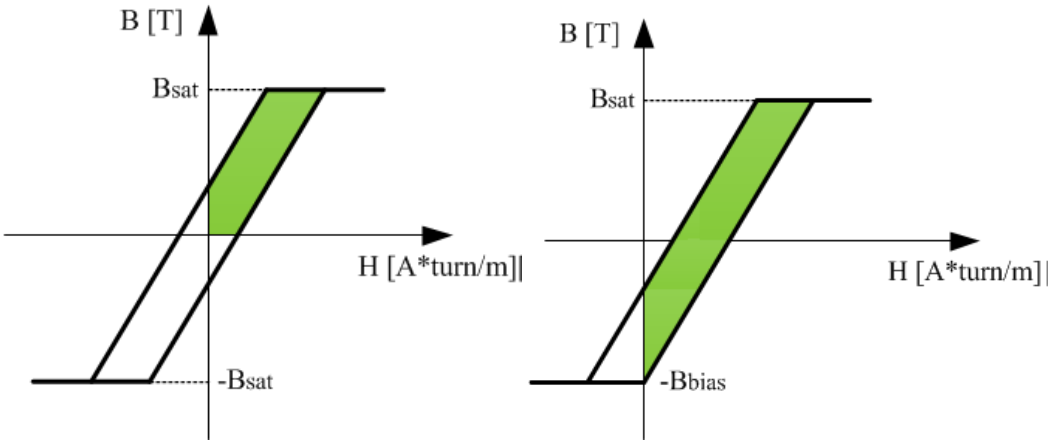

(a) Without PMs (b) With PMs

Figure 2.4: Usable B-H curve range.

energy can be stored in the transformer, as shown in equation (2.3). In this way, the usable B-H curve can be extended to the 3rd quadrant, which helps reduce the amount of magnetic materials needed.

$$B_{eq} = B_w - B_{pm} \leq B_{sat} \tag{2.2}$$

$$B_w \leq B_{sat} + B_{pm} \tag{2.3}$$

A simple design to achieve this is by putting the permanent magnet on the side of the core, as shown in Figure 2.3. The permanent magnet is placed in a direction such that it tries to cancel the flux generated by the windings. With the orientation, permanent magnet is operation where the magnetic field strength excited by the windings and seen by the permanent magnet should be kept smaller than its intrinsic coercive force (H_{ci}). So that permanent magnet will not be demagnetized. Figure 2.4a shows the original usable B-H curve range. Figure 2.4b shows the resulted usable B-H curve range. As can be seen, the usable B-H curve is shifted on the right hand side due to the biased flux generated by the permanent magnets, and thus the usable B-H curve range is extended.

For the two transformer designed proposed earlier, the permanent magnets needed to

fully offset the DC flux is slightly different. And the permanent magnets used for each design is listed in Table 2.2. Distance between the magnets on the top core and the magnets on the bottom core is set to be the same as air gap. So that no virtual air gap will be created and affect magnets performance [8].

Table 2.2: Permanent magnets specifications

Foil winding		
Part number	**Dimensions**	**Quantity**
BZX0X02	$4''$ x $1''$ x $1/8''$	8
BY0X04	$2''$ x $1''$ x $1/4''$	4
Coaxial cable winding		
Part number	**Dimensions**	**Quantity**
BY0X02	$2''$ x $1''$ x $1/8''$	8
BY0X04	$2''$ x $1''$ x $1/4''$	4
BX882	$1.5''$ x $1/2''$ x $1/8''$	8

2.3 Transformer Parametric Circuit Model

As discussed earlier, the high frequency transformer need to achieve low loss, low cost and small size. A interleaved foil winding transformer design with small leakage inductance is proposed. And a FEM model is developed and transformer characterization is also performed to develop a detailed transformer equivalent circuit, shown in Figure 2.5, considering all parasitic elements [9]. Figure 2.6 is the FEM model developed for interleaved foil winding transformer using ANSYS Maxwell.

The high-frequency transformer is unique due to its interleaved windings around a gaped core, and its steady state operation condition. Its core is composed by two AMCC 250 equivalent nanocrystalline core stacked together and gaped at 80 mil (2.03 mm) on the non-coil side. The primary and secondary windings are interleaved and 14 turns each. So this is an one-to-one ration transformer. Also a simplified transformer equivalent circuit is developed and shown in figure 2.5. The one-to-one ratio transformer with galvanic isolation shown in the equivalent circuit model. Each circuit components will be calculated

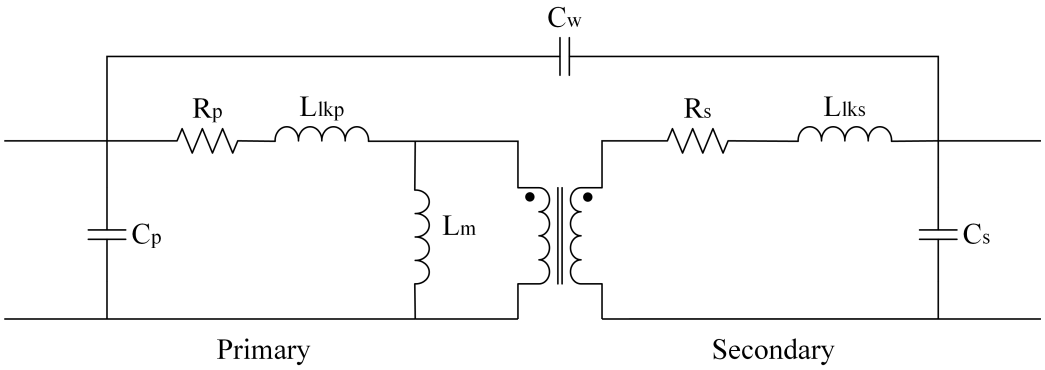

Figure 2.5: Equivalent Circuit of the transformer with isolation

analytically and will be discussed in detail.

In the equivalent circuit model, the magnetizing inductance is represented by L_m and is calculated to be $360\ \mu H$ as shown in equation (2.4). The leakage inductance is represented by L_{kp} for the primary and L_{lks} for the secondary. The total leakage inductance L_{lk} is calculated to be 100 nH as shown in equation (2.5). The equivalent primary and secondary lumped capacitance is represented by C_p, C_s accordingly, which will be hard to calculated. The dc winding resistance, which is the resistance for primary and secondary windings, is represented by R_p and R_s. C_w is the winding-to-winding capacitance. Winding-to-winding capacitance is calculated to be 30 nF according to equation (2.6). DC Resistance R_{DC} is calculated to be $6\ m\Omega$ according to equation (2.7).And primary winding connections are shown on the left side of the figure and the secondary winding connections are shown on the right side of the figure. Saturation current I_{sat} is calculated to be 80 A without any magnets and 160 A with magnets according to equation (2.8). FEM parametric circuit model provides L_m, L_{lk}, C_w, and R_{DC} values. These values has been compared to mathematical calculations.

$$L_m = \frac{N^2}{\Re_c + \Re_g} = \frac{N^2}{\frac{l_c}{\mu A_c} + \frac{l_g}{\mu_o A_c}} \tag{2.4}$$

$$L_{lk} = \frac{4\pi N^2 MLT}{h_c}(\frac{d_w}{3} + d_i) \tag{2.5}$$

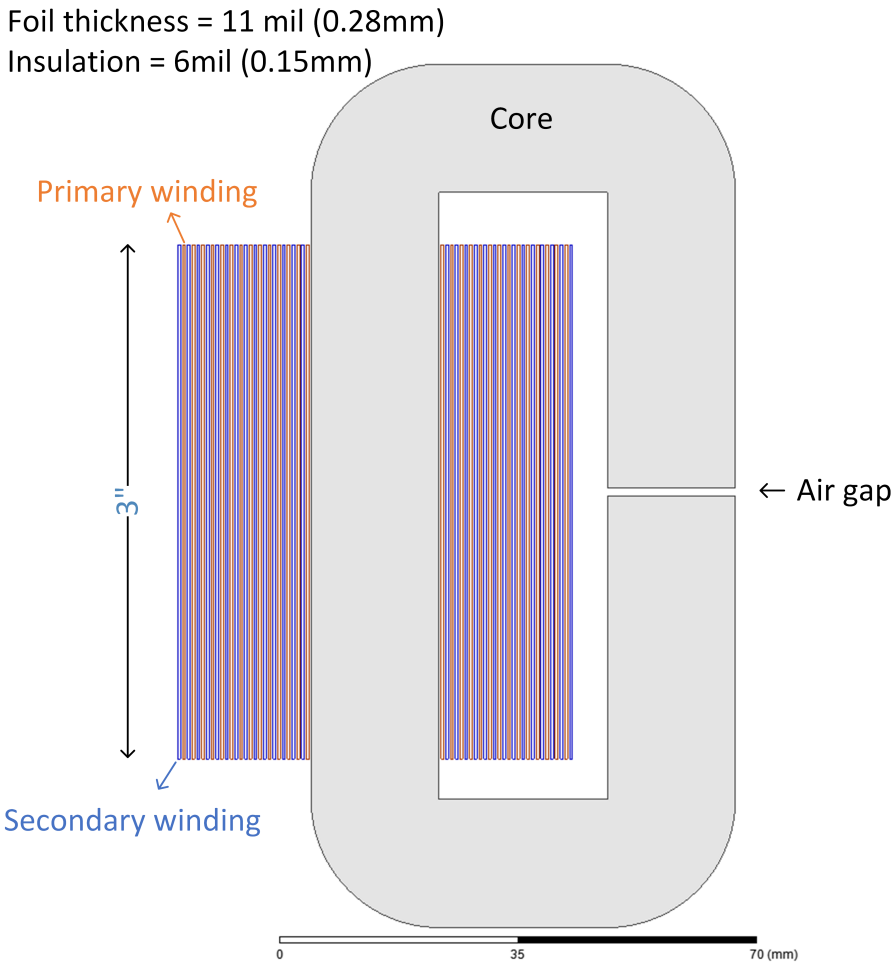

Figure 2.6: Interleaved foil winding transformer

$$C_w = \frac{k\varepsilon_o A}{D} \tag{2.6}$$

$$R_{DC} = \rho \frac{l}{A_w} \tag{2.7}$$

$$I_{sat} = \frac{BA_cN}{L_m} \tag{2.8}$$

2.4 Magnetic Circuit Model

In the S4T, the magnetizing inductance is used as an energy transfer element. The operating cycle starts with one of the bridges charging the transformer from the input source and ends with the other bridge discharging the transformer into the output. These two active states are interspersed with transition states, controlled using the resonant circuits, to ensure soft switching. As shown in Figure 1.2, the total magnetizing current (I_m) is the summation of the the primary input current (I_{pri}) and secondary output current (I_{sec}), and is primarily DC with an AC ripple. However, only one winding will be conducting (active) during the energy transfer period, unlike other solid state transformers. The magnetizing current is the summation of the the primary input current and secondary output current.

The high-frequency transformer of the S4T has an unique feature of DC biased flux. So the transformer size is determined by the maximum flux density of the magnetic core when the design is driven by saturation flux density. When designing the transformer, the peak flux density through the core should be kept below the saturation point of the B-H curve. The design proposed uses permanent magnets to offset the DC flux in core, so that core size can be significantly reduced [10]. Figure 2.8 shows how permanent magnets are added to offset the DC bias in the core. The equivalent magnetic circuit for the transformer design with permanent magnets is shown in Figure 2.7, in which the permanent magnet acts as a constant flux source.

The permanent magnet is placed in a direction such that it tries to cancel the flux generated by the windings. To avoid operating above magnet intrinsic coercive force and get magnets demagnetized, permanent magnets are place on the side of the core leg as shown in Figure 2.8 and Figure 2.3. The permanent magnets used are magnetized through the thickness. Interleaved foil winding have been simplified, but the direction of the current has been identified. The flux generated by the winding Φ_w is counter-clockwise. The flux generated by the permanent magnet should have a reverse direction to cancel it. So the top

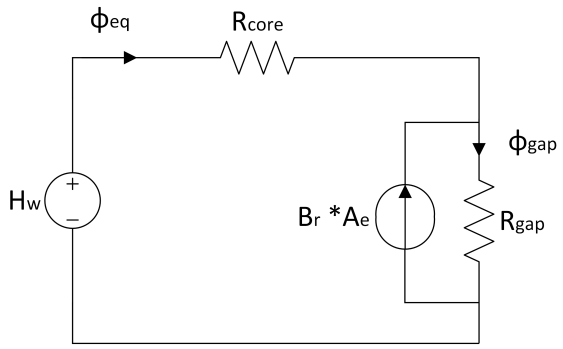

Figure 2.7: Equivalent magnetic circuit for the transformer design with permanent magnets

of the core magnetic core need to be north pole and bottom of the magnetic core need to be south pole, since flux travels from south to north inside the magnetic material. Therefore, for the permanent magnets mounting on the top of core, south pole should be facing toward the core. For the permanent magnets mounting on the bottom of core, north pole should be facing toward the core. In this way, permanent magnets create a flux flowing path as shown in the Figure 2.3, which tends to cancel the flux generated by the winding. The cross section area of the two permanent magnet should be the same as the core A_e such that enough biased flux is generated. Magnets are places on all four side of the non-winding core leg, so that best performance can be achieved.

FEM simulation is performed for the transformer design with and without the permanent magnets. The interleaved foil winding is simplified. Current excitation into the winding is sinusoidal AC current at 16 kHz. The excitation creates the same flux in the core as the actual foil winding transformer is excited with 60 A average magnetizing current. The region of the model is set to be $\pm 100\%$ in x,y,z directions. The boundary condition constrains the field inside the core and winding. Fine mesh is being applied to only the core. And the total number of elements in the solution is greater than 60,000. The simulation results are shown in Figure 2.9. As shown in the results, with the same excitation, the design with permanent magnets has a much lower flux density due to the permanent magnets flux cancelling effect. It also shows that flux density are high on the corners and

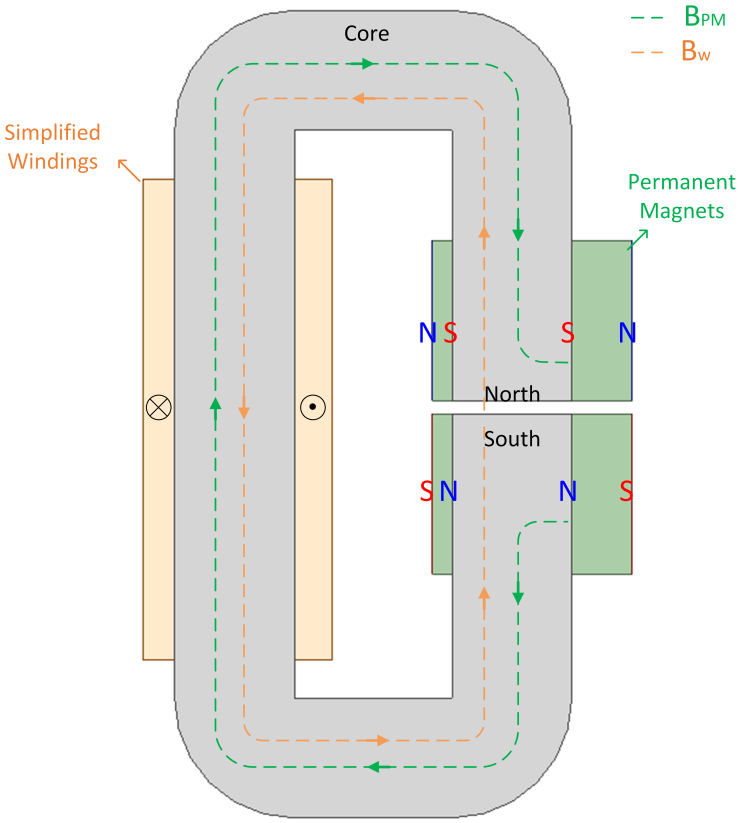

Figure 2.8: Transformer design with permanent magnets to offset DC bias

near the air gap.

2.5 Transformer Characterization

Double pulse test (DPT) is a standard test for device characterization.[11] The test analyzes the impact of parasitic inductance and capacitance on switching performance of devices. However, DPT is now utilized to perform transformer characterization. The test setup is shown in Figure 2.10. DPT is very useful to experimentally measure the transformer parasitic components and compare values with analytically and FEM values. In this section, transformer magnetizing inductance, leakage inductance and saturation current will be measured.

DPT test setup is shown in Figure 2.10. and circuit function diagram of the test fixture is shown in Figure 2.12. The output of a 0 120 V_{ac} variable transformer is stepped up through

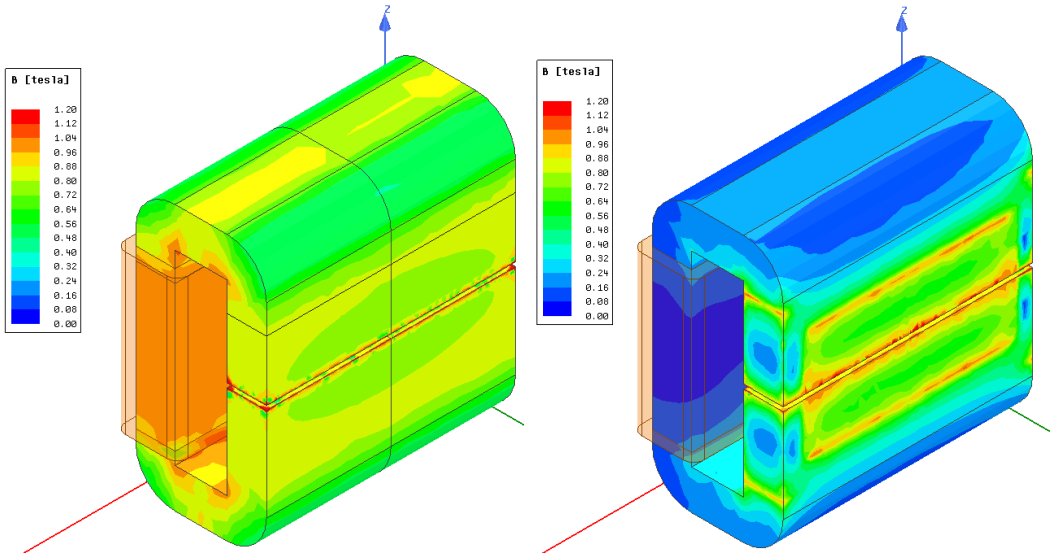

(a) Without permanent magnets (b) With permanent magnets (PM not shown)

Figure 2.9: Finite element analysis simulation of two transformer designs at 60A excitation

a transformer with a turns ratio of 1:5, which is then connected to a full bridge rectifier and electrolytic capacitors to provide 0∽1000 V_{dc} voltage for device switching operation. The high-side switch S2 and low-side switch S2 is controlled by a double-pulse signal (V_{Gs1}, V_{Gs2}), and the theoretical voltage and current waveforms of DUT (V_L, I_L) are shown in Figure 2.11. The time instants t1 and t2 are the moments to characterize the turning-on and turning-off conditions of the DUT. The voltage and current levels at switching instants of the Device Under Testing (DUT) can be controlled by changing the variable transformer′s output and the first charging duration t1.

Saturation Current

As discussed in earlier sections, the permanent magnets are used to offset the DC flux bias in the core, so that the flux ripple can utilize more core to storage energy. It is designed that the permanent magnets can boost the saturation current by 100%. However the experimental tests show that it can only achieve a 86% improvement in saturation current. FEM models in ANSYS Maxwell have been built to analysis the cause. However research has shown that FEM results and experimental results have a mismatch and accurate calculation

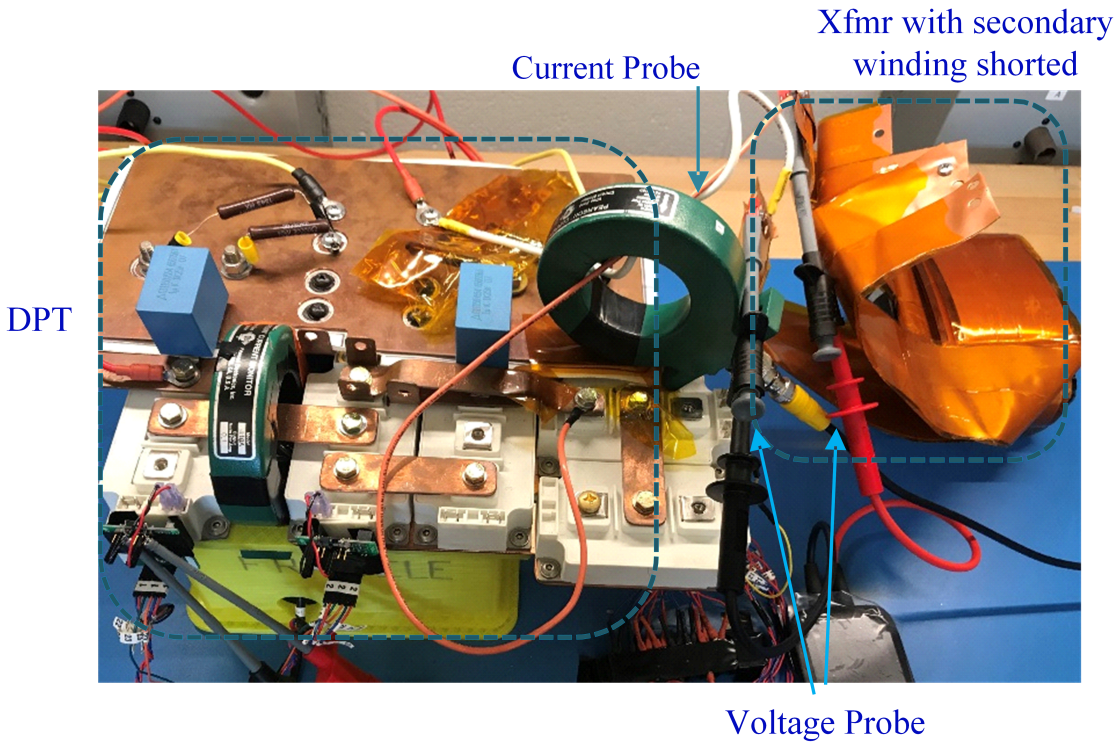

Figure 2.10: Double Pulse Test (DPT) Setup

of the core loss under dc bias conditions is still a challenge [12].

Foil winding transformer has been tested for saturation current with and without permanent magnets. So how much energy can be stored in the core can be measured by what is the peak current that can be input into the core before it saturates.

Transformer is first tested without magnets. Only one winding is connected to the test setup, the other winding is left as open circuit. Figure 2.13 shows the test results. Figure 2.13a shows the voltage across the transformer winding and current through the transformer winding. The knee point of the current waveform is the saturation current of the transformer. The magnetizing inductance is calculated using equation (2.9). Figure 2.13b shows the calculated magnetizing inductance vs. current plot. The designed and measured magnetizing inductance is 350 μH. In this way, it is easier to determine the

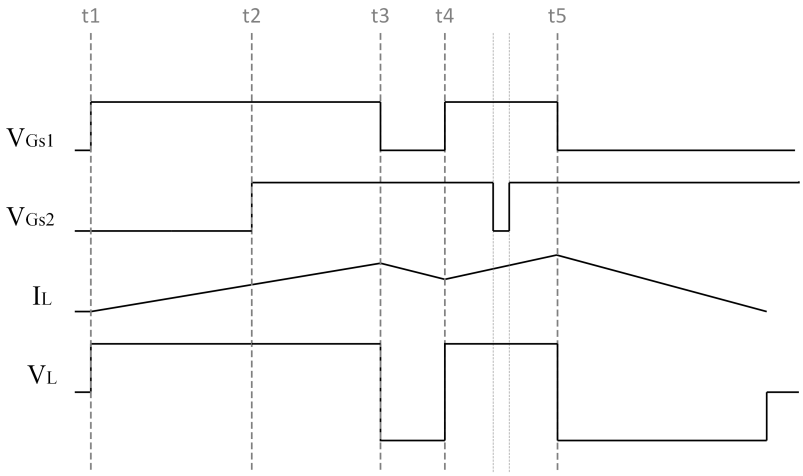

Figure 2.11: Theoretical gate signal voltage and current waveform

saturation current of the transformer without magnets to be 75 A.

$$V = L_m \frac{di}{dt} \tag{2.9}$$

Then transformer with permanent magnets mounted as shown in Figure 2.3. Figure 2.3 shows the test results. Figure 2.14a shows the voltage across the transformer winding and current through the transformer winding. Figure 2.14b shows the calculated magnetizing inductance vs. current plot. The magnetizing inductance is 350 μH. In this way, the saturation current of the transformer with magnets is determined to be 145 A. Experimental result shows that the magnets are able to increase the saturation current by 93%.

2.6 Conclusion

Two HF transformers designed with foil winding and coaxial winding are evaluated through simulation and experimental results. Both transformers use the nanocrystalline core from MK Magnetics, but with different winding design. Also the foil winding transformer design with and without magnets are evaluated through simulation and experimental results. Transformer characterization result are provided as well. DPT tests have been preformed on the transformer with and without magnets, the saturation current results show

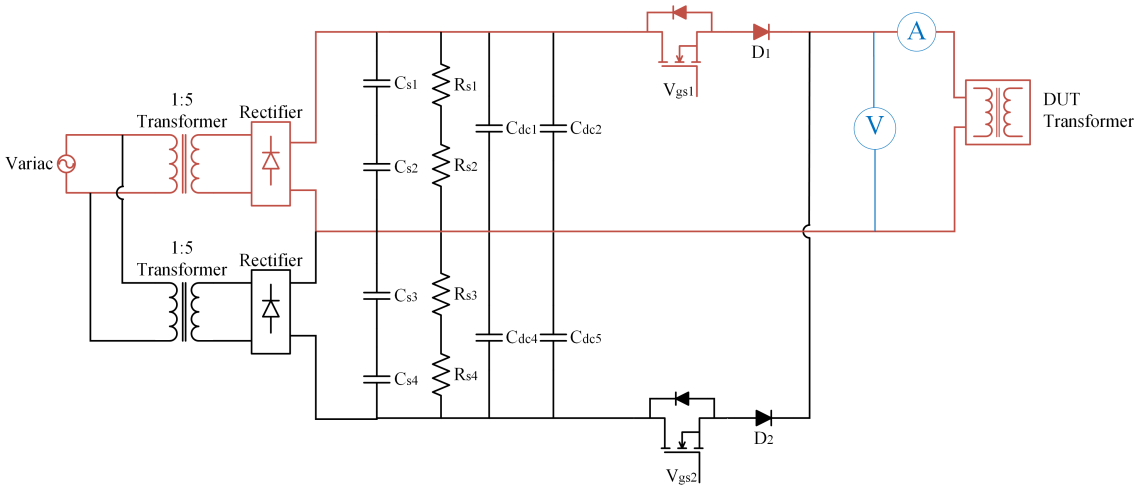

(a) Charging

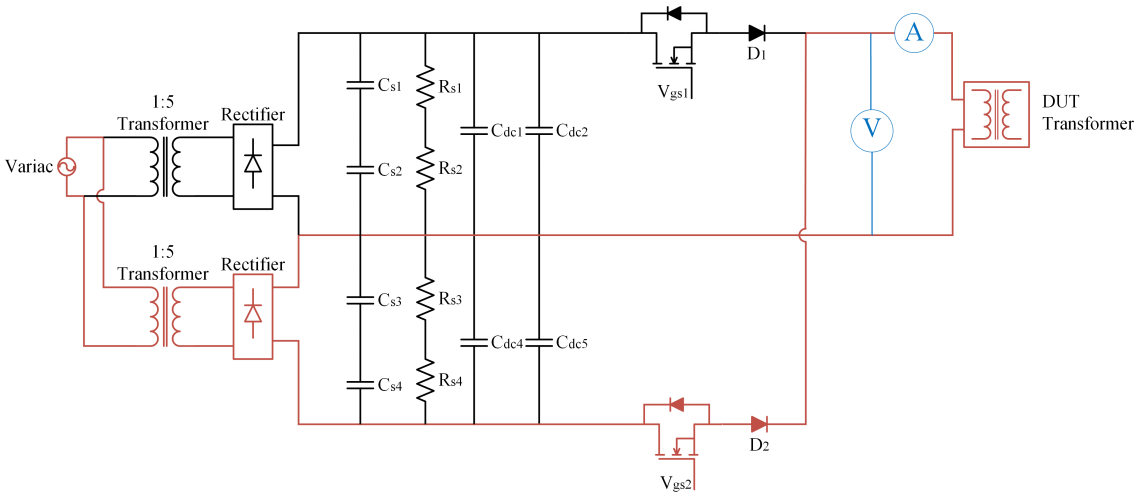

(b) Discharging

Figure 2.12: DPT Test Circuit Operating Principles

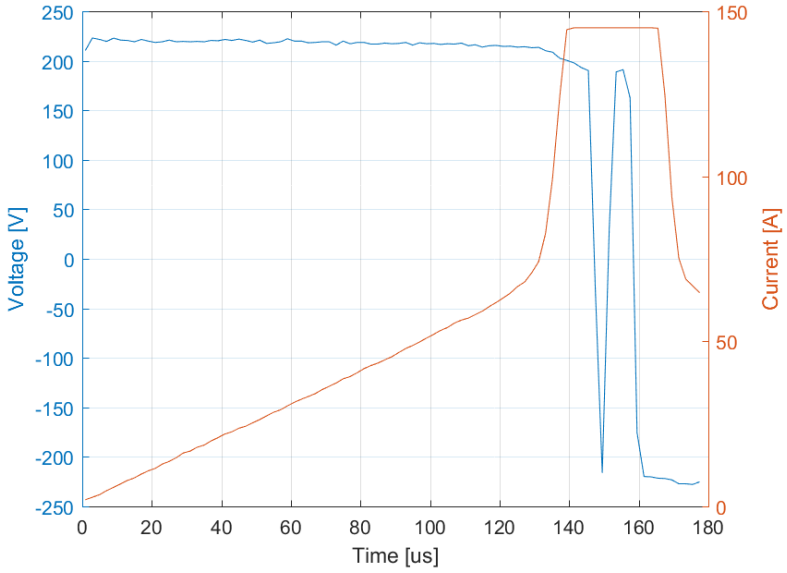

(a) Voltage and current waveform of DUT

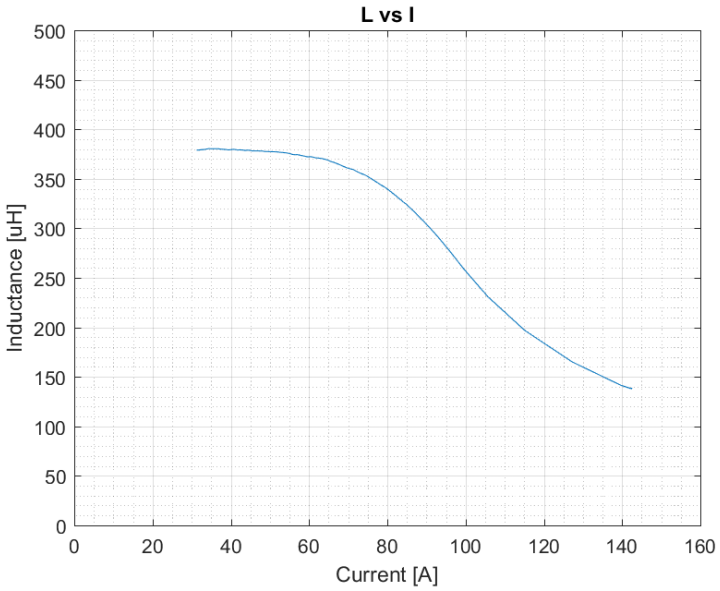

(b) Calculated magnetizing inductance

Figure 2.13: DPT results of foil winding transformer without magnets.

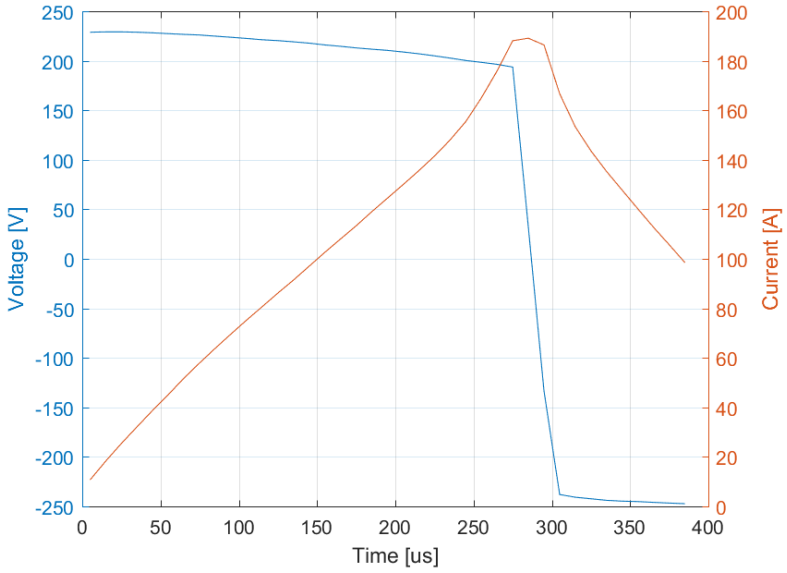

(a) Voltage and current waveform of DUT

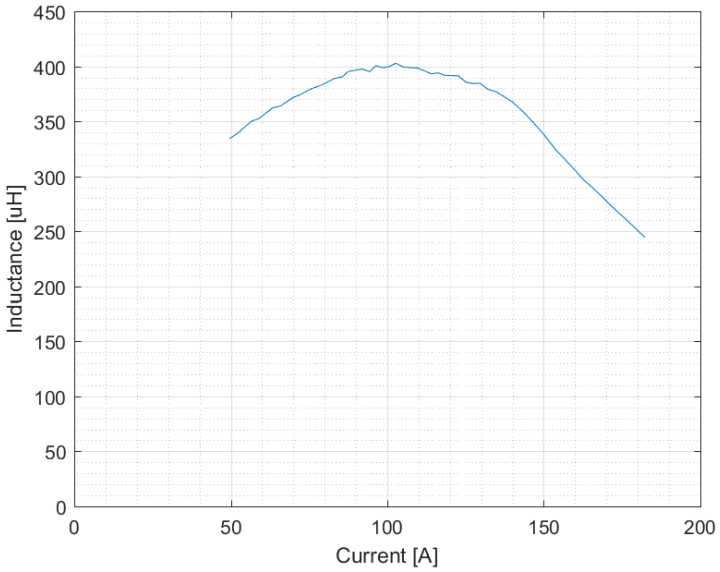

(b) Calculated magnetizing inductance

Figure 2.14: DPT results of foil winding transformer with magnets.

that design with permanent magnets can store much more energy than the conventional transformer. The permanent magnets can improve the saturation current level by 90%. And the distance between the magnets on the top core and on the bottom core should be set to air gap, so that no virtual air gap will be introduced and affect magnet performance.

CHAPTER 3
COPPER LOSS

3.1 Introduction

The high frequency transformer is a critical component of any solid state transformer. In the case of S4T, the HF transformer is similar to a flyback transformer with the addition of transition stages, resulting in some atypical operating modes. Only one winding is active during the active energy transfer time. However, there is significant proximity effect induced eddy current losses in the inactive winding [13]. During the transition times, both the windings are carrying very high frequency currents (10-20 times switching frequency) resulting in significant AC copper loss even though the transition period is small (5-10% of switching period). This chapter explains the nature of these eddy currents in the open winding and during transitions stages, which are unique to S4T, and presents analysis to evaluate these losses. Mathematical derivations to calculate these unique AC losses are presented. FEM analysis to verify the analytical method is presented. Finally, an experimental method to evaluate the transformer loss is presented.

3.2 Winding Copper Loss Calculation in Active and Open Winding During Energy Transfer States

3.2.1 AC Current Distribution in S4T windings

The AC current distribution in a typical transformer non-interleaved winding is shown in Figure 3.1a. The eddy currents caused by proximity effect result in both positive and negative currents in the same winding, though the sum of these current is always equal to I, the current flowing out of the terminals. The effect of these eddy currents increases with the number of layers. The current distribution is symmetric across primary and secondary

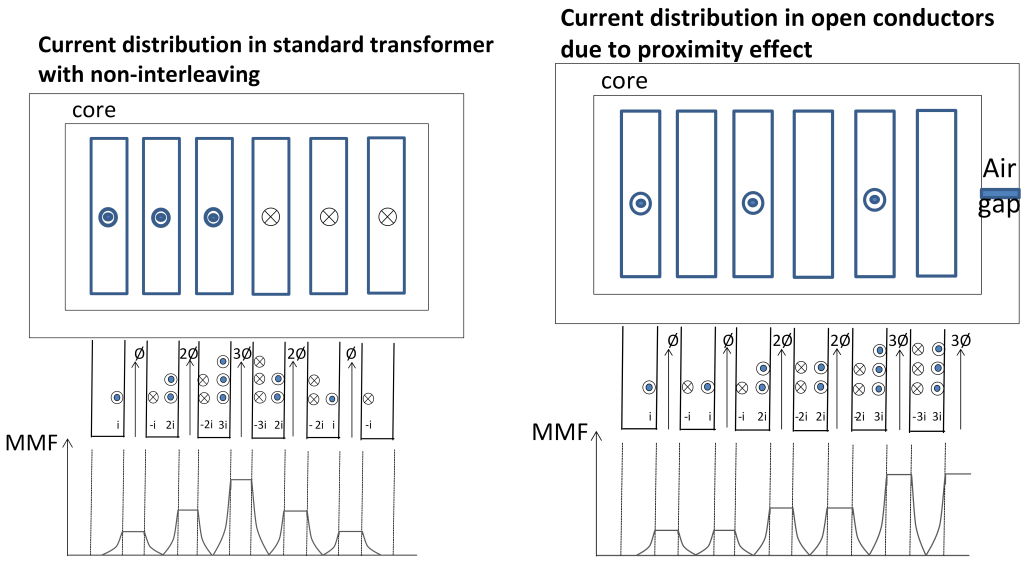

(a) in a standard transformer (b) in S4T

Figure 3.1: AC current distribution.

windings.

Similar analysis can be extended to the S4T transformer, where the windings are interleaved to keep the leakage inductance low. The current distribution in active windings, shown in Figure 3.1b, is similar to the current distribution in one of the windings of a standard non-interleaved transformer. However, there are eddy currents in the open windings, which appear as positive and negative currents at the winding edges. Please note that the effective sum of these eddy currents is zero, as the winding is open at its terminals. Interestingly, the eddy currents in the open windings of the S4T are worse than the eddy currents in the standard non-interleaved transformer. If the windings are not interleaved in S4T, the current distribution in the open windings will be (-3i, 3i) in all the layers. In a standard transformer, the HF currents are reduced by interleaving the windings. In S4T, even with interleaving, the current distribution is worse than a standard non-interleaved transformer. Hence, the eddy current loss calculation is much more significant in the case of S4T.

3.2.2 AC Resistance Factor and Loss Calculation of Active Winding

The AC resistance factor, R_{fac}, for the active windings can be calculated using the standard Dowell′s equation (3.1) [14].

$$R_{fac} = G1 + \frac{2}{3}(N^2 - 1) * G2 \tag{3.1}$$

$$G_1 = \Delta \frac{\sinh 2\Delta + \sin 2\Delta}{\cosh 2\Delta - \cos 2\Delta} \qquad G_2 = \Delta \frac{\sinh \Delta - \sin \Delta}{\cosh \Delta + \cos \Delta} \tag{3.2}$$

$$\Delta = \frac{foil\_thickness}{\delta}, \delta = \frac{7.6}{\sqrt{f}} \tag{3.3}$$

where δ is the penetration depth calculated at switching frequency. The AC loss in the active windings is calculated using equation (3.4), where D is the active energy transfer time.

$$AC\_loss_{cond} = (\frac{I_{pp}}{2} * 0.577)^2 * R_{fac} * R_{dc} * D \tag{3.4}$$

3.2.3 AC Resistance Factor and Loss Calculation of Open Winding

The AC resistance factor calculation for the open windings, R_{fac_open}, is not readily available in literature, unlike the R_{fac} for active windings. Hence an approximate method based on current density distribution in a conductor is proposed to calculate the AC resistance factor for the open windings. The current density distribution in the active winding and the open winding at different Δ is shown in Figure 3.2.

The proximity effect results in both positive and negative currents, though the effective sum is equal to the current flowing out of the winding terminal. The current density is typically exponential in nature, decreasing as we move from surface of the conductor to the center [15]. At higher Δ, the positive and negative currents are presented at opposite

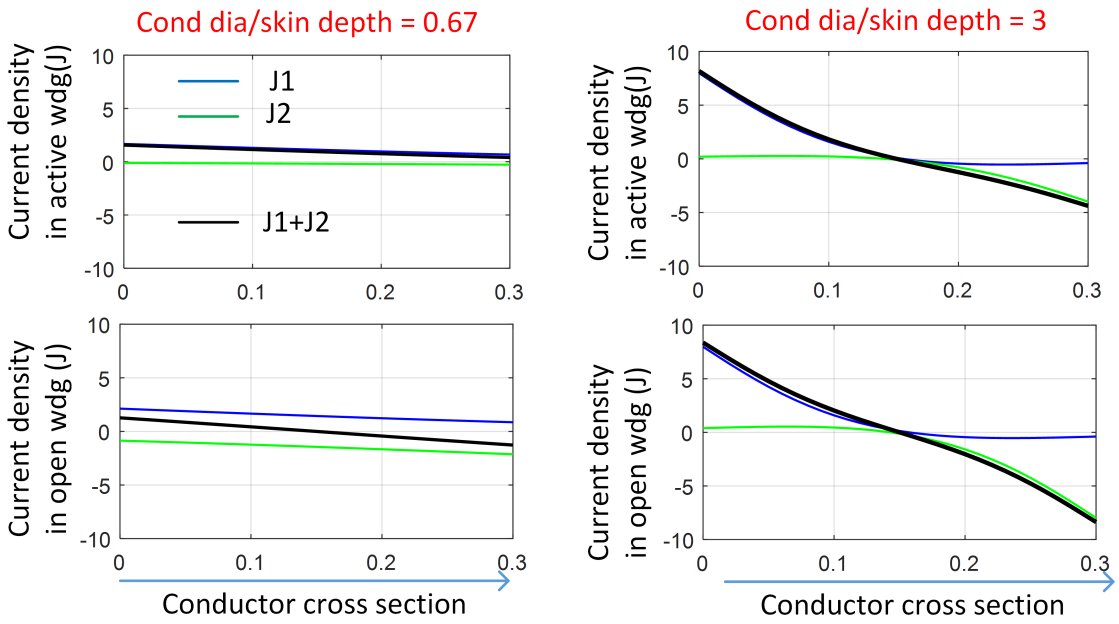

Figure 3.2: Current distribution in active winding and open winding at different Δ.

conductor surfaces. As Δ decreases, the positive and negative currents combine, resulting in a more uniform current distribution across the conductor. Hence, the loss and the effective AC resistance factor increases with Δ. The current distribution in any N^{th} layer of an active winding is given by equation (3.5).

$$J_1 = \frac{N-(0.35N)k}{|mean(A)|}A \qquad J_2 = \frac{-(N-1-(0.35N)k)}{|mean(B)|}B \tag{3.5}$$

$$A = e^{-\frac{d}{\delta}}e^{-\frac{jd}{\delta}}, \quad B = e^{-\frac{D-d}{\delta}}e^{-\frac{j(D-d)}{\delta}}, \quad k = 1-\tanh(2(\Delta-1)) \tag{3.6}$$

The AC resistance factor for the N^{th} layer is calculated by equation (3.7).

$$R_{fac\_active} = mean(|J_1+J_2|^2) \tag{3.7}$$

The effective AC resistance factor for an N layer winding is the mean of the AC resistance of all N layers [16]. The results of the proposed method and the Dowell′s equation for the active windings are compared in Figure 3.3a. The proposed method follows the

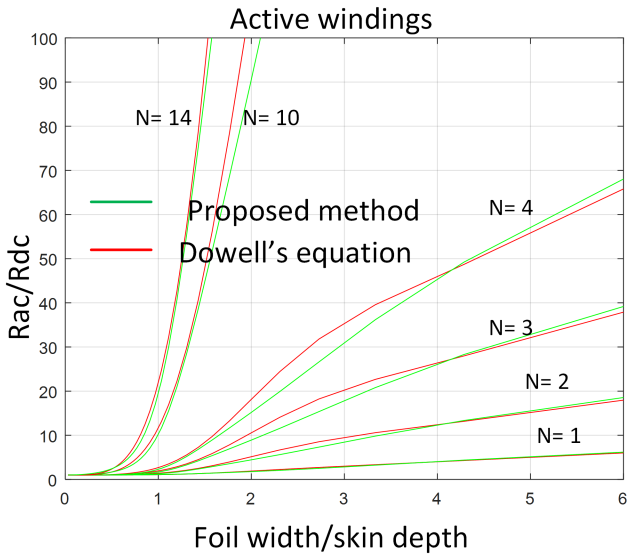

(a) Comparison of AC resistance factor for the active windings calculated using proposed method and Dowell′s equation.

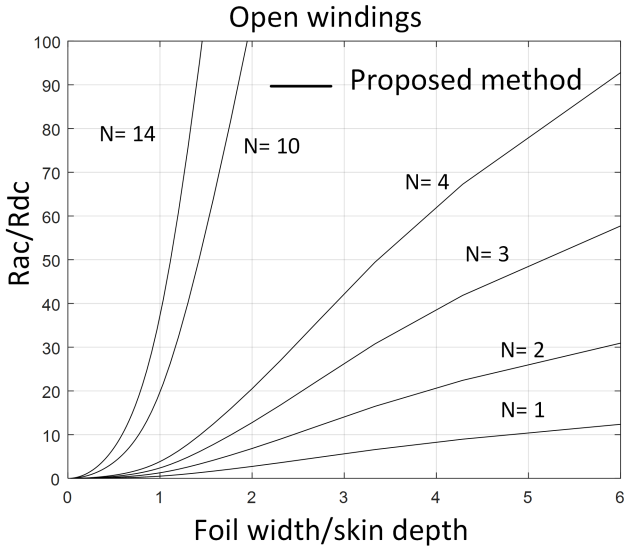

(b) AC resistance factor for the open windings calculated using the proposed approach based on current density distribution.

Figure 3.3: AC resistance factor

Dowell′s equation within acceptable error of $< 10\%$.

The method is now applied to find AC resistance factor of the open windings. For the open windings, the positive and negative current density distribution, J_1 and J_2 respectively, are given by equation (3.8).

$$J_1 = \frac{1 - 0.15k}{|mean(A)|}A \quad J_2 = \frac{1(1 - 0.15k)}{|mean(B)|}B \tag{3.8}$$

The AC resistance factor of open windings with N layers is given by equation (3.9) and in shown in Figure 3.3b.

$$R_{fac\_open} = \frac{(N+1)(2N+1)}{6} mean(|J_1 + J_2|^2) \tag{3.9}$$

It can be seen that the AC loss in open windings may dominate the AC loss in active windings, especially in thicker conductors. The AC loss in the open windings is calculated using equation (3.10).

$$AC\_loss_{open} = (\frac{I_{pp}}{2} * 0.577)^2 * R_{fac\_open} * R_{dc} * D \tag{3.10}$$

3.3 Verification of Loss in Open winding using FEM analysis

To verify the loss in the open (inactive) winding, FEM analysis has been performed in ANSYS Maxwell environment. The model of the transformer used for the FEM analysis is shown in Figure 3.4. The copper foil of 2 mm is used to simulate the winding consisting of 5 primary and secondary turns. The primary (orange) and secondary (violet) are interleaved but the current is present in only secondary winding.

Please note that only AC current is simulated here, though the actual S4T transformer will have both DC and AC components. The magnetic field (H) measured along the axis shown in (redline) in Figure 3.4, is shown in Figure 3.5. The H filed increases as we move towards the core. The increase and decrease of the H filed along the axis indicates

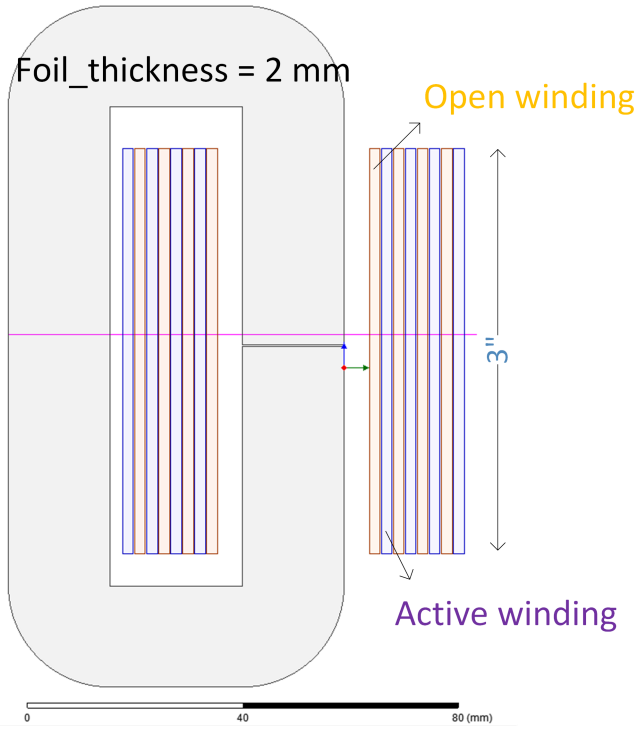

Figure 3.4: Model used to evaluate eddy current distribution and losses in open winding of S4T transformer in ANSYS Maxwell.

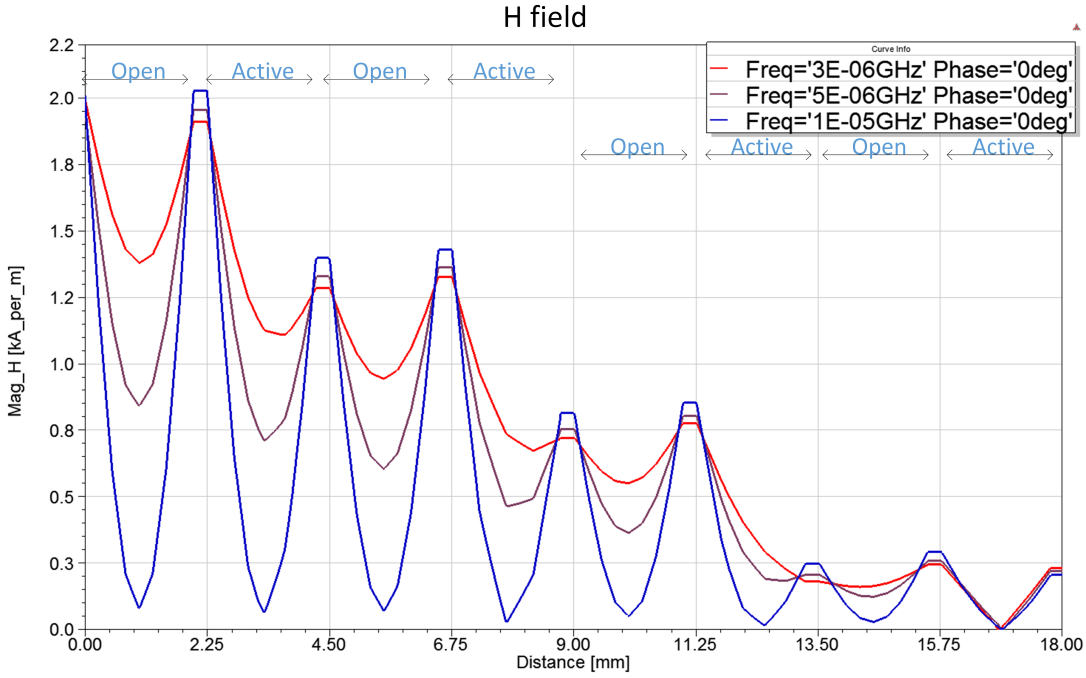

Figure 3.5: The magnetic field (H) measured along the axis, redline shown in Figure 3.4.

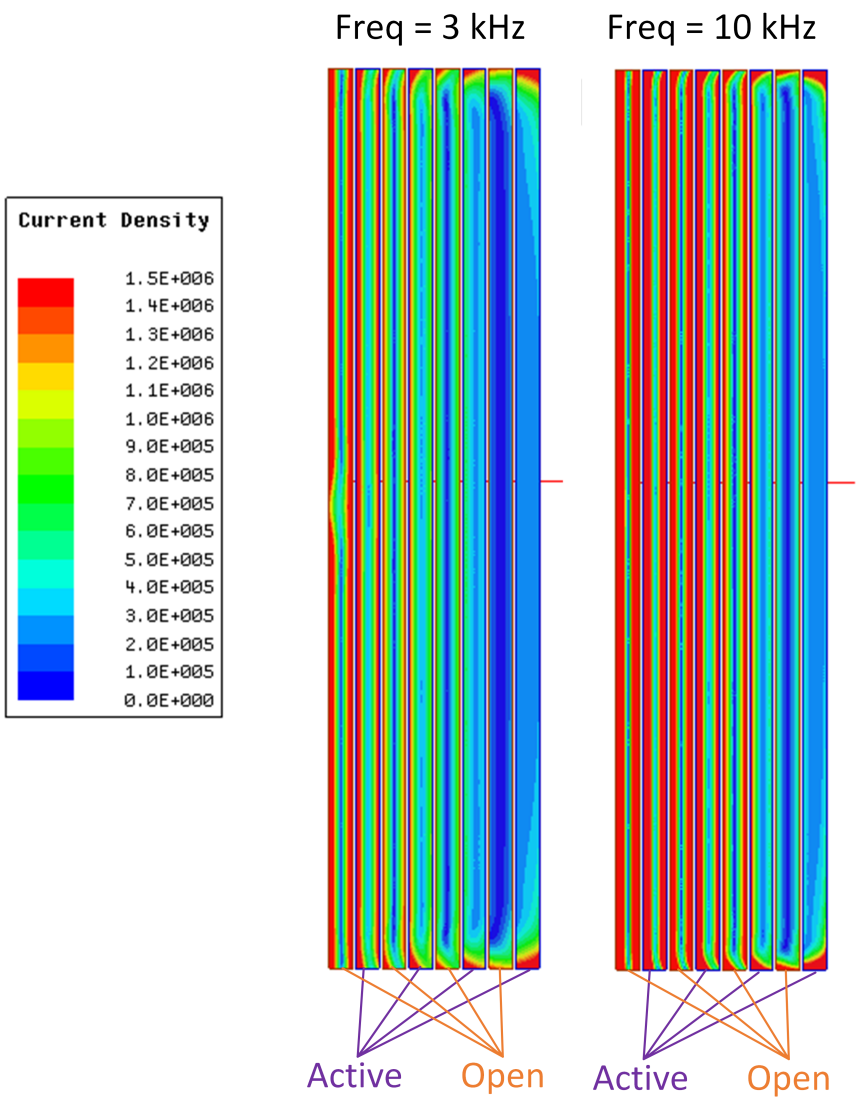

Figure 3.6: Current density plots across the windings for 3kHz and 10kHz.

the presence of negative currents. The variation in H increases as the frequency increase, indicating the increase in eddy currents. Across an active winding, there is an effective increase in H, as we move towards the core. However, across an open winding the effective H remains the same because the positive and negative currents cancel out resulting in zero current at the winding terminals.

The current density plots are shown in Figure 3.6 for two different frequencies. There are two observations. First one is the presence of eddy currents in the open winding. The eddy currents in any open turn are higher than the eddy currents in the corresponding turn

of the active winding. The second observation is the increase in the eddy currents with frequency in both the active and open windings.

The current density distribution along the axis (red line) shown in Figure 3.4, is plotted in Figure 3.7. As seen in the figure, the active winding has both active and negative currents, as indicated by the phase. Similarly, there are positive and negative currents in the open windings. As explained in the previous section, the effective AC current in the open winding is always higher than the corresponding AC current in the active winding. It can also be seen that the effective current in open winding is zero, as the terminals are open.

The current density distribution shown in Figure 3.7 is used to calculate the AC resistance factor for both the open windings and the active windings. The results for the active windings are shown in Figure 3.8a. The AC resistance factor for the active windings compares well with the Dowell′s equation confirming the FEM analysis setup. The AC resistance factor for the open windings derived from FEM analysis, shown in Figure 3.8b, compares well ($< 10\%$ error) to that the values derived using proposed equation (3.10) in the previous section, thereby, verifying the proposed method. The error between the FEM results and the proposed method could be because of the eddy currents induced by the leakage flux from the transformer air gap.

3.4 Winding Copper loss calculation during transition states

Transition stages are the states during which the converter moves from one active voltage vector to the other with a controlled dv/dt (determined by resonant capacitors C_{r1}, C_{r2}). As shown in Figure 3.9, during the transition the current flows in both the windings. The primary and secondary currents vary such that the sum is equal to magnetizing current, I_m. The currents vary at a frequency determined by the transformer leakage inductance, L_{lkg1} & L_{lkg2} and resonant capacitors, C_{r1} & C_{r2}. The AC resistance factor can be calculated using equation (3.11) with the penetration depth calculated at frequency determined by the

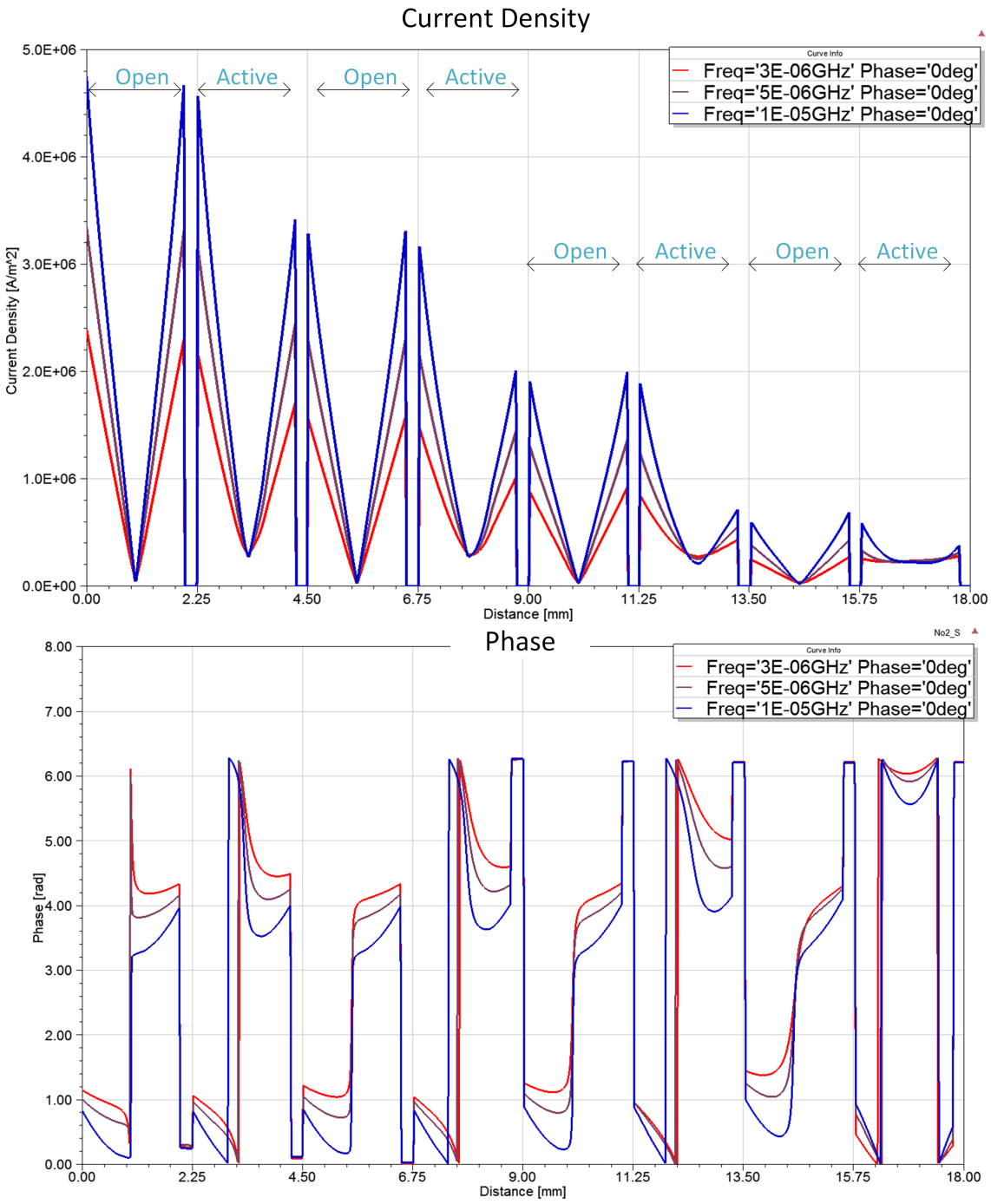

Figure 3.7: Current density magnitude and phase distribution measured along the axis in Figure 3.4

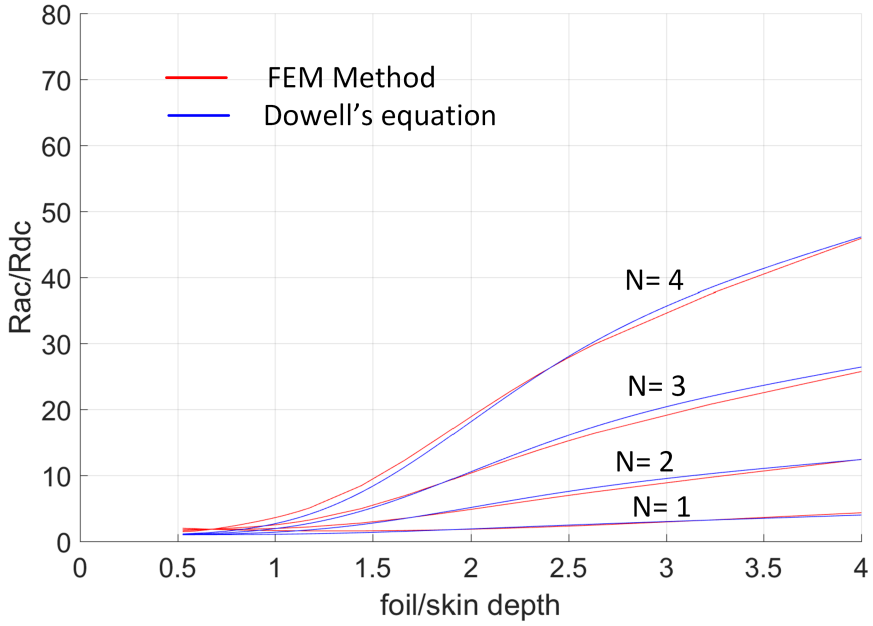

(a) Comparison of AC resistance factor for the active windings using FEM method and Dowell′s equation.

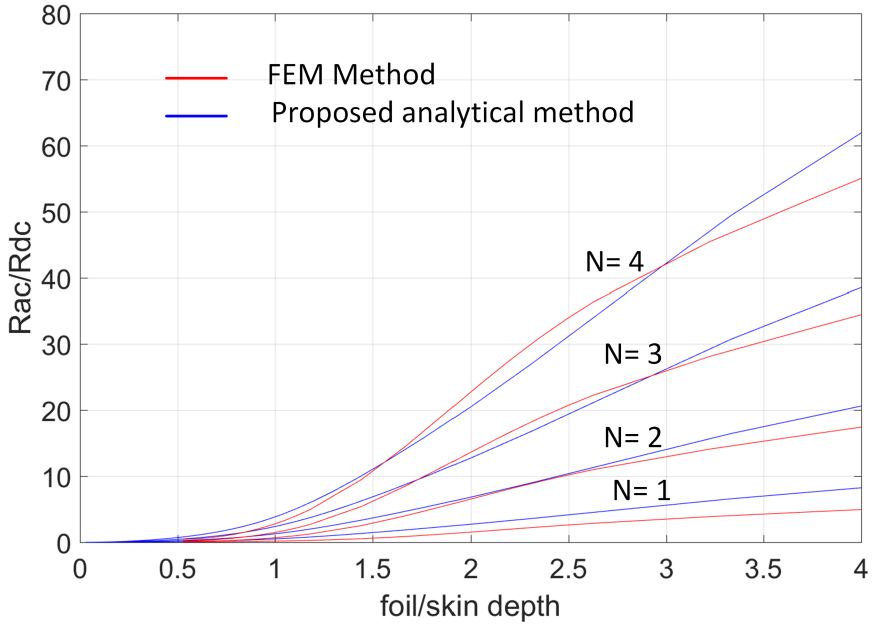

(b) AC resistance factor for the open windings using FEM method and proposed analytical method.

Figure 3.8: AC resistance factor

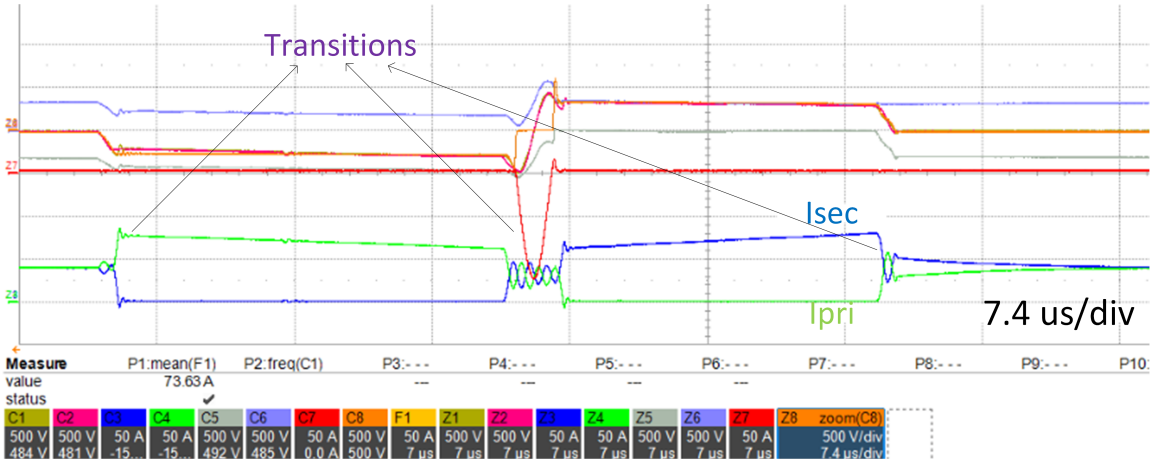

Figure 3.9: Primary and secondary current during transition state.

resonate frequency of L_{lkg1} + L_{lkg2} and C_{r1} + C_{r2}.

$$R_{ac_{trans}} = \Delta \frac{\sinh 2\Delta + \sin 2\Delta}{\cosh 2\Delta - \cos 2\Delta}, \qquad \delta = \frac{7.6}{\sqrt{F_{tr}}} \tag{3.11}$$

Please note that during the transition, the transformer winding interleaving aids in reducing the effective AC resistance (N=1). The AC loss in the windings during transition is calculated using equation (3.12), where D_{tr} is transition time of the switching period (typically 5-10%), determined by the dv/dt and the voltage difference between the most positive vector and the most negative vector.

$$AC\_loss_{trans} = 2(\frac{I_{pp}}{1.414})^2 * R_{ac\_trans} * R_{dc} * D_{tr} \tag{3.12}$$

3.5 Experimental Tests

Experiments are carried out to confirm the AC losses in the windings against the loss calculated using FEM methods and proposed analytical method. In order to separate the copper loss from core loss in measurement, transformer cores are removed. The experiment test setup is shown in Figure 3.10.

Two set of tests are performed to measure AC loss in active winding and in open wind-

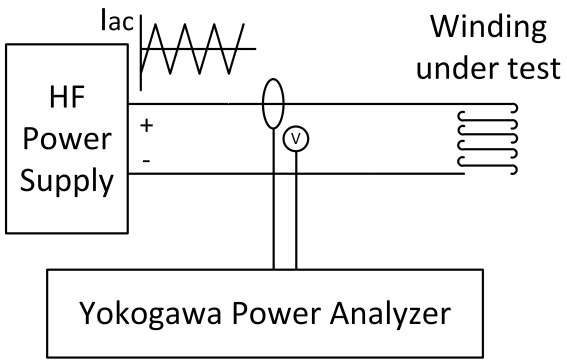

Figure 3.10: AC copper loss measurement test setup.

ing. AC copper loss during transition stage occurs at much higher frequency, and therefore will not be measured using current setup. First set of test is performed on the copper foil windings contain both primary winding and secondary winding. Second set of test is performed on the copper foil windings contain only primary winding. In both tests, primary winding is the active winding and is connected to a high frequency power supply with a series connected inductor. The HF power stage is a simple half-bridge controlled with a fixed 50% duty cycle and fixed 30 kHz switching frequency. A triangle-wave current will be energized into the active winding. The voltage and current across the active winding are measured using a high precision Yokogawa power analyzer (WT1806E with 5MHz bandwidth) coupled with a high precision LEM current sensor (IT 60-S) to determine the AC copper loss.

AC copper loss will be measured on winding sets with number of turns vary from 12 turns to 1 turn. As Figure 3.3 and Figure 3.8 has shown, AC resistance factor vary with N, number of turns, and D, which is foil thickness/skin depth. Therefor, AC copper loss will be measured on winding sets with number of turns vary from 12 turns to 1 turn. And foil thickness of 22 mil and 11 mil copper will be tested. At each measuring point, different current ripple will be apply for accuracy.

AC resistance factor for active winding and open winding are shown in Figure 3.11. Figure 3.11a shows that the measurements matches up with FEM method and Dowell′s

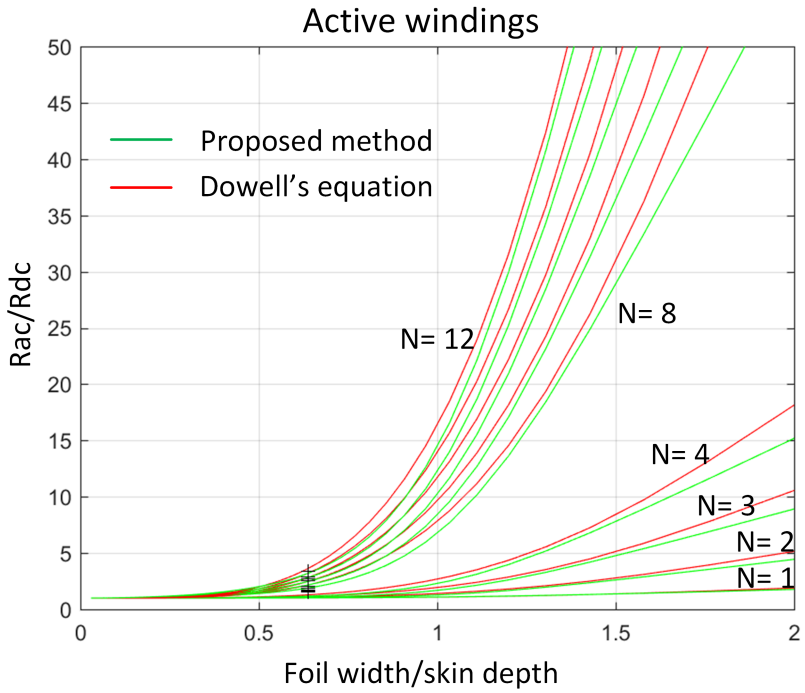

(a) Comparison of AC resistance factor for the active windings using experimental results, FEM method, and Dowell′s equation.

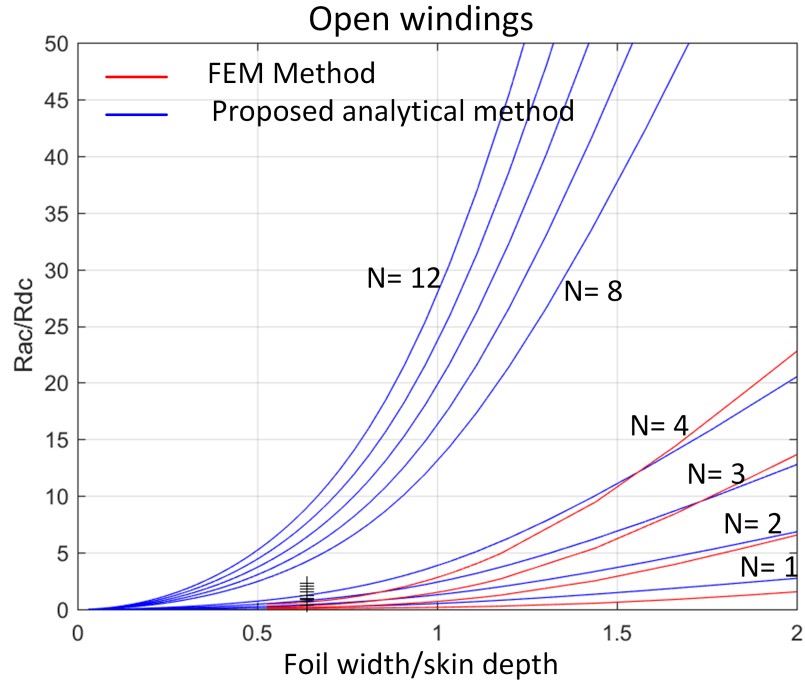

(b) AC resistance factor for the open windings using experimental results, FEM method, and proposed analytical method.

Figure 3.11: AC resistance factor

equation for active winding. Figure 3.11b shows that the measurements matches up with FEM method and proposed analytical method for opening winding. So both FEM results and experimental results show that the proposed method for AC copper loss in active winding is accurate.

Figure 3.12a shows the AC resistance factor as number of turns increases in the active winding at foil width/skin depth = 0.64. Figure 3.12b shows the AC resistance factor as number of turns increases in the open winding at foil width/skin depth = 0.64. At lower number of turns, the measurement results for the active winding is larger than analytical methods but within 20% error margin. This is could be caused by measurement errors due to DC resistance is really small at lower number of turns. The actual power loss measured by Yokogawa is very small, especially at lower number of turns. So the experimental results does not match up the analytical method very well at lower number of turns. However, for the same foil width/skin depth, AC resistance factor increase exponentially with number of turns. That is as expected. For open winding, the measurement results are much lower than analytical methods, especially at higher number of turns. Even though the AC copper loss in the open winding are smaller than expected, it is still as much as the AC copper loss in the active winding. So the AC winding loss in open winding is still significant in AC winding losses.

3.6 Loss estimation for a 25 kVA 480/480 V S4T

A 25 kVA 16 kHz transformer for a 3-phase 480 V S4T application was designed to meet the specifications presented in Table 3.1. The core loss is estimated using Steinmetz equation.[2] The effect of DC offset is neglected for this analysis. The transformer design is optimized across various parameters such as total loss, leakage inductance, parasitic capacitance, cost, size (core area x window area) for various combinations of turns and magnetizing inductance L_m. The results of the multi-objective design is shown in a radar plot in Figure 3.13.

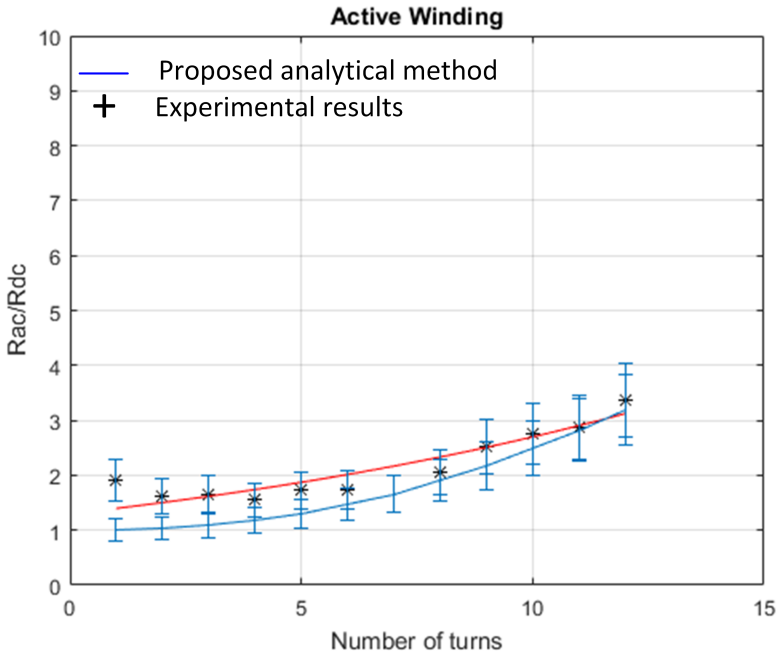

(a) Active winding

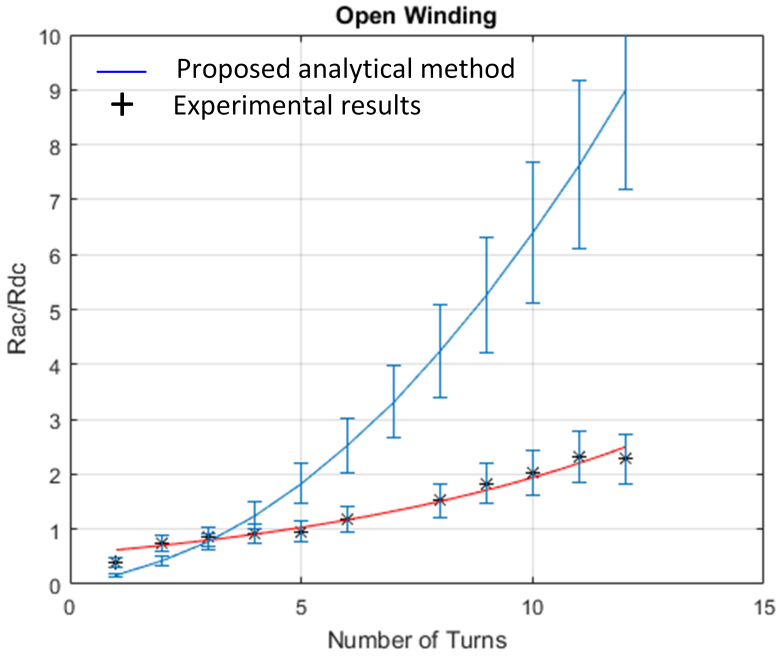

(b) Open winding

Figure 3.12: Experimental result of AC resistance factor

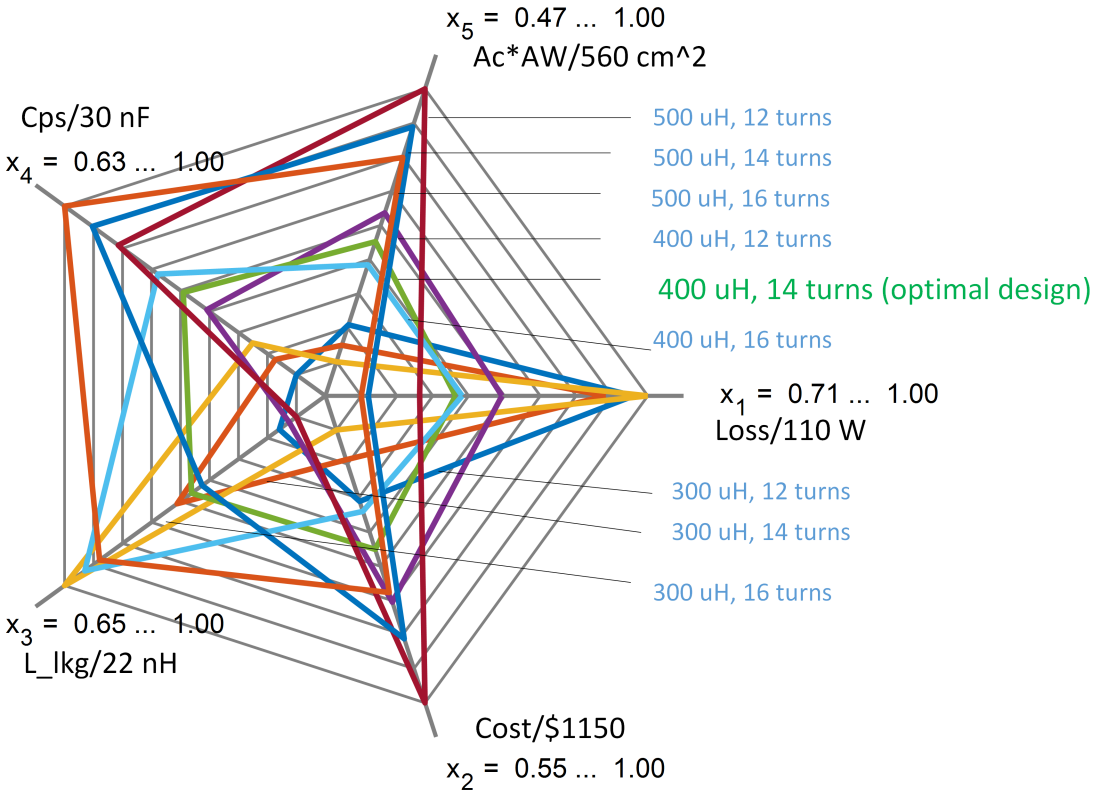

Figure 3.13: Multi-objective S4T transformer design.

Table 3.1: Specification of HF transformer.

Parameter	Value	Parameter	Value
kVA	25	Insulation	Kapton 3 mil
Voltage	480 V_{rms}	Foil	3" x 0.011"
Switching frequency	16 kHz	Core	SC2061M1
Loss	<0.5%	Magnetizing inductance	200-400 μH
Avg. mag. current	95A	Leakage inductance	<1% of L_m
Current ripple	$< 0.6\ I_{m,avg}$	Inter-winding cap.	<1 nF

The design with magnetizing inductance of 400 μH and 14 turns satisfies all objectives optimally. Similar design is performed for 20 kHz and 25 kHz to study the impact of switching frequency, F_{sw}, on the transformer losses and the results are presented in Figure 3.14a. The transformer losses tends to increase with F_{sw}, primarily because of the increase in the copper loss. The core loss increases only slightly with F_{sw}. Even though the increase in F_{sw} causes loss density of the core to increase, the required L_m decreases resulting in a much smaller core and hence only a small increase in loss. The copper loss consists of DC and AC losses. With increase in switching frequency, the active duty cycle reduces, resulting in higher average I_m and higher DC loss. Across the three designs, the AC current ripple I_{pp} is maintained at 30% of I_{m_avg}. At 16 kHz, the AC loss is 50% of DC copper loss, but at 25 kHz, the AC copper loss is higher than the DC copper loss. AC losses increase at faster rate because of the increase in Δ with switching frequency.

The breakdown of the AC copper loss is shown in Figure 3.14b. The AC copper loss is dominated by transition loss and loss in the open windings. With the increase in F_{sw}, the transition time becomes a major part of the switching cycle and hence an increase in the loss. The loss in the open windings is almost twice as that of the active windings at 25 kHz because of the increase in Δ. The results indicate the importance of identifying the open winding loss and transition loss in the S4T.

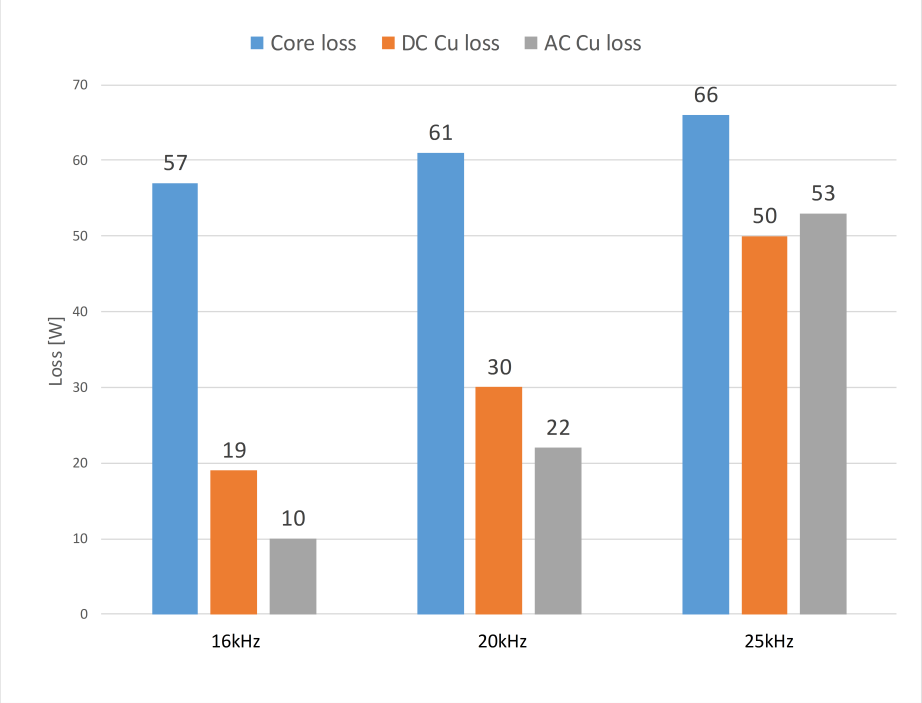

(a) core loss and copper loss

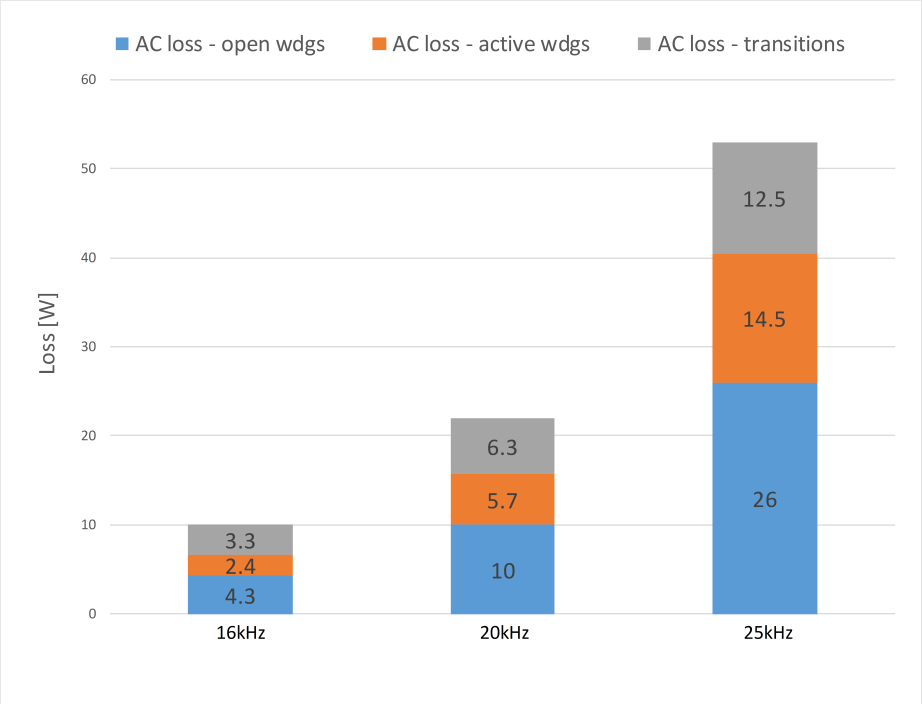

(b) Breakdown of AC copper loss

Figure 3.14: Loss estimation for 25 kVA 480 V/480 V S4T transformer at different frequencies.

3.7 Conclusion

This chapter presented unique AC copper loss that can occur in the soft-switching solid state transformer. It was shown that the active winding could induce eddy currents in the open transformer windings resulting in AC copper loss, even though no current is present at the winding terminal. Also, it was shown that though the transition times are a much smaller part of the switching cycle, the loss during this period can be significant because the winding currents during this period vary at very high frequency. Detailed analytical methods to estimate these losses are presented. The effect of induced eddy currents in open windings in verified through FEM analysis in ANSYS Maxwell environment. In addition, the proposed analytical method was verified using FEM analysis. Using an example transformer design, it was shown that the loss in the open (inactive) windings could be higher than the loss in the active windings and tend to increase with number of turns and frequency. In S4T, even though the AC current is relatively small ($< 30\%$ of the DC current), the eddy currents in the open windings could result in a significant AC copper loss, especially at higher frequencies.

CHAPTER 4
CORE LOSS

4.1 Introduction

Numerous power electronics topologies rely on magnetics operating with a DC flux bias. This is the case of the well-known DC-DC Boost converter, flyback converter, and more recently several solid-state transformers topologies such as the Soft-Switching Solid-State Transformer (S4T) [17]. Many studies have shown that core losses increase significantly under DC bias conditions [4][18]. For soft magnetic materials, typically used in high-performance, medium-frequency applications, up to a 2-3x increase in core losses under large DC bias, at constant flux density ripple, has been typically reported [19][20]. The increase has been shown to be independent of the flux density ripple frequency, for the frequency range of interest in medium power conversion, and highly non-linear on the DC flux bias .

Nanocrystalline soft magnetic material is a fairly new development. This material is promising to have the best overall performance over a broad range of frequencies when compared to other available materials [21]. ItâĂŹs relatively high saturation flux density, combined with its incredible low loss and high permeability through a wide frequency range, makes it useful in many applications [21]. To develop a unique high frequency transformer, it is necessary to thoroughly characterized the core loss of nanocrystalline core for different flux density ripple under several DC flux bias. The characterization shows an unprecedented 4.3x increase under DC bias when compared to no DC bias conditions, at constant flux density ripple. Further, the relative increased in the losses have been shown to be more significant at lower flux ripple. These results have been carefully analyzed and confirmed through several direct and indirect measurements and will be presented in this

Table 4.1: Core specifications

Manufacture	MK Magnetics	A	79 mm
Material	Nanocrystalline	B	128 mm
Part Number	SC2062M1	D	50 mm
Net Area A_e	11 cm^2	E	22 mm
B_{sat}	1.1 T	F	35 mm
Mass	2170 g	G	85 mm

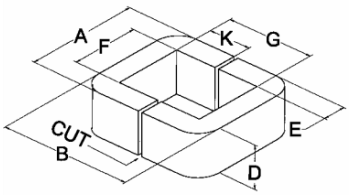

Figure 4.1: C-core dimension standard

chapter. The core loss measured experimentally under no DC bias will be presented first and compared to the theoretical losses from the Steinmetz equation [22] and the improved generalized Steinmetz equation (iGSE) [23]. Experimental results under different DC flux bias and for different flux density ripple will be detailed next.

4.2 Test setup

Two main manufacture of nanocrystalline cores are MK magnetics [24] and Hitachi [21]. A set of nanocrystalline Vitroperm C-cores (SC2062M1) from MK Magnetics has been tested. It consists of two half cores has shown in figure 4.1. The main characteristics of the core are summarized in Table 4.1.

The test setup is shown in Figure4.2. Three windings are placed around the core under test (CUT). The first winding is the 3 turns AC excitation winding and is connected to the output of the high frequency power supply. The HF power stage is a simple half-bridge

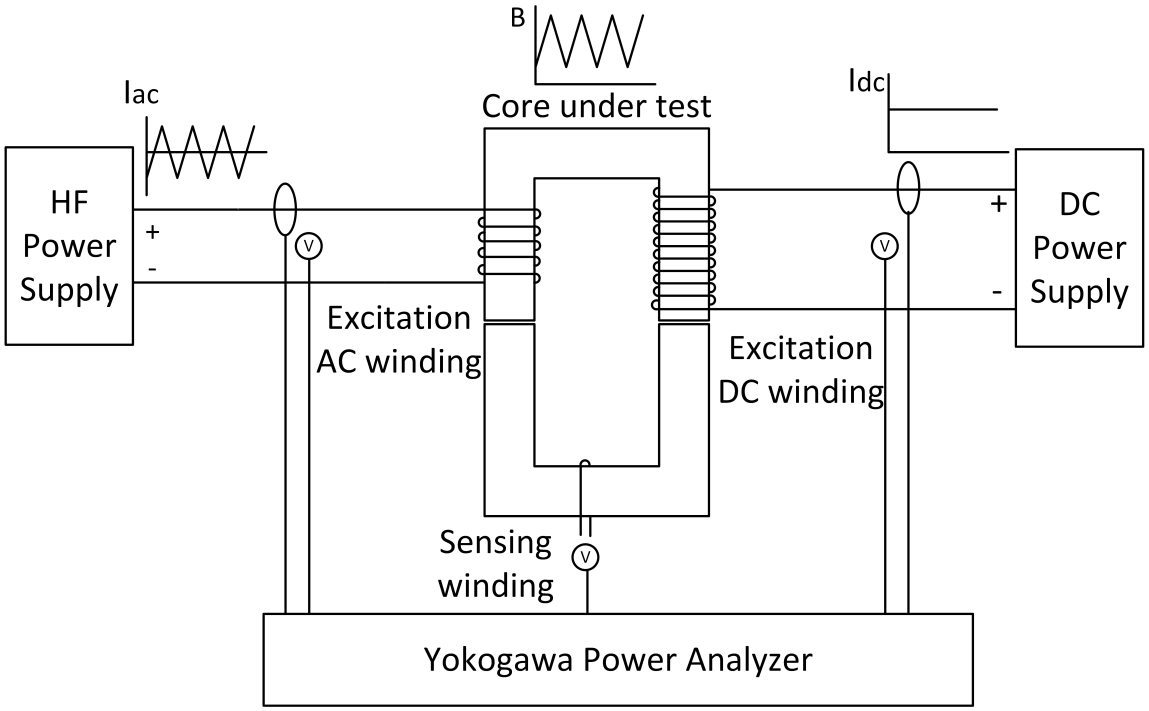

Figure 4.2: Test setup

controlled with a fixed 50% duty cycle and fixed 30 kHz switching frequency. It outputs a symmetrical triangular current through the winding. The secondary winding is the 10 turns DC excitation winding and is connected to the output of the DC power supply. DC power supply output a pure DC current into the winding which creates DC flux bias in the core. The third winding is a single-turn, sensing winding wound on the opposite leg of the core to sense the flux density flowing through the CUT. The flux density B flowing through the core can be expressed from the voltage measured across the sense winding V_{sense} as in equation (4.1).

$$B(t) = \frac{1}{A_e} \int_0^t V_{sense}(t)dt \tag{4.1}$$

The voltage and current across the excitation windings are measured using a high precision Yokogawa power analyzer (WT1806E with 5MHz bandwidth) coupled with a high precision LEM current sensor (IT 60-S) to determine the core loss level. The triangular flux ripple in the CUT is controlled by varying the voltage of the HF power supply between

70 V_{ac} to 120 V_{ac}. The exact flux flowing through the core, accounting for any leakage flux from the AC excitation winding, is determined from equation (4.1) using the sense winding. The number of turns is kept low and a single-layer winding is used so as to neglect any proximity effect in the winding. Similarly the AC excitation winding is made out of Litz wire to minimize the AC resistance of the winding, measured at $R_{ac,AC} = 31\ m\Omega$ at 30 kHz. DC excitation winding is 12AWG stranded wire, resistances are measured to be $R_{dc,DC} = 20.8\ m\Omega$ and $R_{ac,DC} = 2.9\ \Omega$ at 30 kHz.

4.3 Core Loss without DC Bias

The core loss are measured first under no DC flux bias conditions and for different flux density ripple using the experimental setup shown figure 4.2. Figure 4.3 shows the test waveforms with 3 turns on the AC excitation winding , and a peak-to-peak current of I_{pp}=24 A. The sensing winding square wave peak voltage is (V_{sense}) =16.9 V. Using equation (4.1) this gives a peak-peak flux density ripple at ΔB = 256 mT. For this operating point, the total loss level measured from the power meter is $P_{(tot\_mea)}$ = 9.8 W. This corresponds to the sum of the core loss and the winding loss due to the AC resistance of the winding, at the switching frequency. The AC loss are calculated at $P_{AC\_winding} = \frac{R_{ac,AC} I_{pk}^2}{3}$ = 1.5 W. The core AC loss at this flux density ripple level are then: $P_{core\_measured} = P_{tot\_mea} - P_{AC\_winding}$ = 8.3 W.

Table 4.2 summarizes the results for different ΔB_{pkpk} in the core following the same method. It should be noted that peak-to-peak current in the winding does not directly fix the flux density ripple in the core as the number of turns of the primary and the airgap are varied to achieved the target induction as detailed above.

The measured core losses are also compared to the expected losses from the Steinmetz equation, $P_{steinmetz}$, and the improved generalized Steinmetz equation (iGSE) [], P_{iGSE}, for non-sinusoidal excitation using the Steinmetz coefficient provided by the manufacturer. As expected $P_{steinmetz} > P_{core\_measured}$ as the flux ripple is not sinusoidal, which leads to

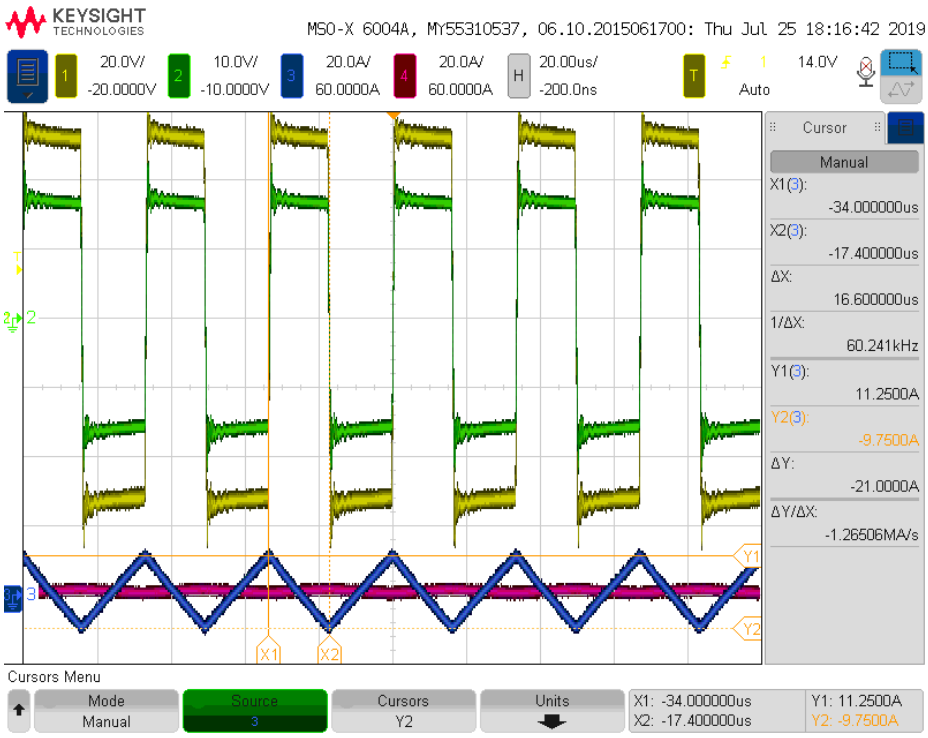

Figure 4.3: Test waveform for ΔB_{pp}=250 mT at B_{DC}=0 T

Table 4.2: Measured core losses without DC bias for different ΔB

ΔB_{pkpk} (mT)	208	256	340	512	558	634	818
I_{pkpk} (A)	20.8	24	22.7	26.5	20.3	40.5	52.3
$P_{tot\_measured}$ (W)	7.2	9.8	14.2	29.7	35.1	48.7	78.9
$P_{winding}$ (W)	1.1	1.5	1.3	1.8	1.1	4.2	7.0
$P_{core\_measured}$ (W)	6.1	8.3	12.9	27.9	34.1	44.5	71.9
$P_{steinmetz}$ (W)	6.7	10.1	17.7	39.7	47.1	60.6	100.4
P_{iGSE} (W)	5.9	8.9	15.6	35.2	41.7	53.7	88.1
$\epsilon(P_{core\_mea} - P_{iGSE})$	3.3%	-6.4%	-17.4%	-20.7%	-18.4%	-17.1%	-18.4%

an overestimation of the losses from the Steinmetz equation. As expected, the iGSE for triangular excitation gives lower losses than the conventional Steinmetz equation, yet the measured core losses are still lower, with a consistent relative error of 20% when compared to P_{iGSE}. This is due to the variability in the typical Steinmetz coefficient provided by the manufacturer and confirms that the experimental setup is not adding any additional losses from measurement errors. Figure 4.4 shows the measured and expected losses for different ΔB under no DC bias.

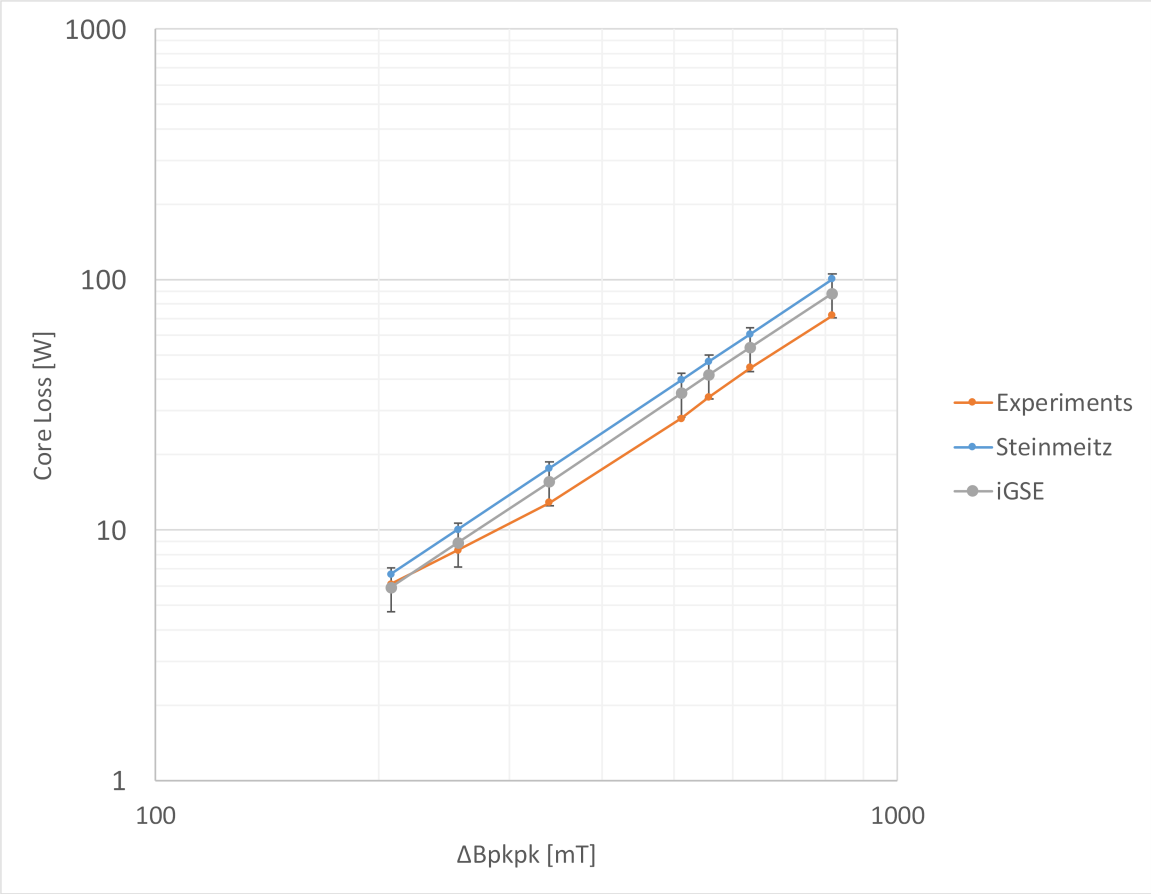

Figure 4.4: Measured core losses compare to Steinmetz and iGSE for different ΔB_{pkpk} at no DC bias

4.4 Core Loss with DC Bias

The same core tested with no DC flux bias in the previous section is tested with different DC bias in the following. To do so, the same test setup than in the previous section is used, with the exception that a secondary DC excitation winding is added to the core and connected to a controllable DC current source through a large inductor to avoid any AC current in this winding that would create additional losses. Test setup is shown in Figure4.2. For this series of tests, AC flux density ripple and DC flux density bias are varied independently by controlling the AC and DC power supplies voltage and current, respectively.

Yokogawa power analyzer measures the voltage and current across the AC and DC excitation winding. The resistance of the windings are measured using LCR meter (Hioki IM3533). AC resistance of the AC excitation winding is $R_{ac,AC} = 31\ m\Omega$, and the AC resistance of the DC excitation winding is $R_{ac,DC} = 2.9\ \Omega$,measured at 30 kHz. DC resistance of the DC excitation winding is $R_{dc,DC} = 20.8\ m\Omega$. Therefore the core loss can be determined by using equation (4.2).

$$P_{core\_loss} = P_{AC\_mea} - P_{AC\_winding} + P_{DC\_mea} - P_{DC\_winding} \tag{4.2}$$

The measured core losses for different peak-peak flux density ripple and under different DC flux density bias B_{dc} are plotted in Figure 4.6a. This shows that at constant ΔB, the core losses start increasing starting at $B_{dc} \sim$ 0.4 T, that is at $B_{dc} \sim \frac{B_{sat}}{3}$. This is better shown in Figure 4.6b by the displacement factor (DPF), first introduced in [], and essentially defined as the core losses normalized to the zero DC offset condition losses: DPF = $\frac{P_{core,withbias}}{P_{core,nobias}}$. DPF factors as high as 4.3 have been measured, what is significantly higher than what has been reported for nanocrystalline, usually in the range of 2-3 []. Similarly to what was reported for ferrite material, the DPF is larger for lower ΔB, meaning that the relative core losses increased under DC bias is more significant at lower flux density

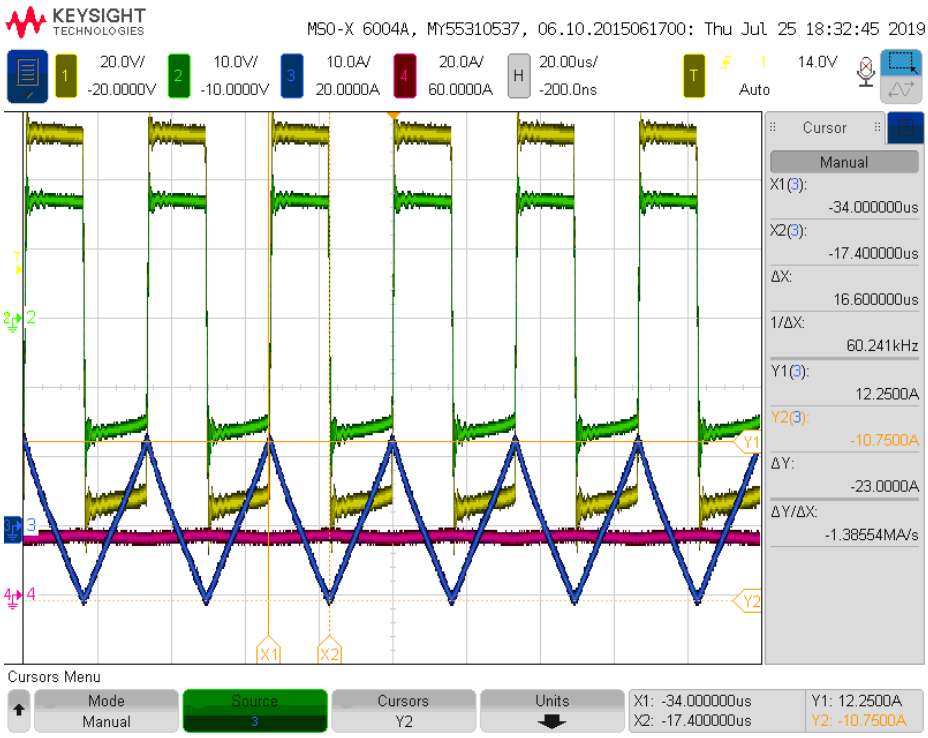

Figure 4.5: Test waveform for ΔB_{pp}=250 mT at B_{DC}=0.8T

ripple. This is a significant finding that has not been reported for nanocrystalline material to the author′s knowledge, and could be valuable in the optimal design of magnetics based on soft-magnetic materials.

4.5 Discussion

Soft magnetic materials are widely recognized as a prime choice for designing magnetics in high performance power electronics applications, yet the impact of DC flux bias on the core losses is not well understood and probably underestimated. This chapter reports an unprecedented 4.3x increase in the core loss of nanocrystalline material, under non-saturated core conditions, and typical flux ripple conditions (<30%) power electronics. Further, the relative core losses increase has been shown to be larger at lower flux density ripple. These results have been confirmed through multiple direct and indirect measurements and for several cores of the same material. Though the physical origin of these increased losses is not entirely understood, the potential fallouts apply to any topol-

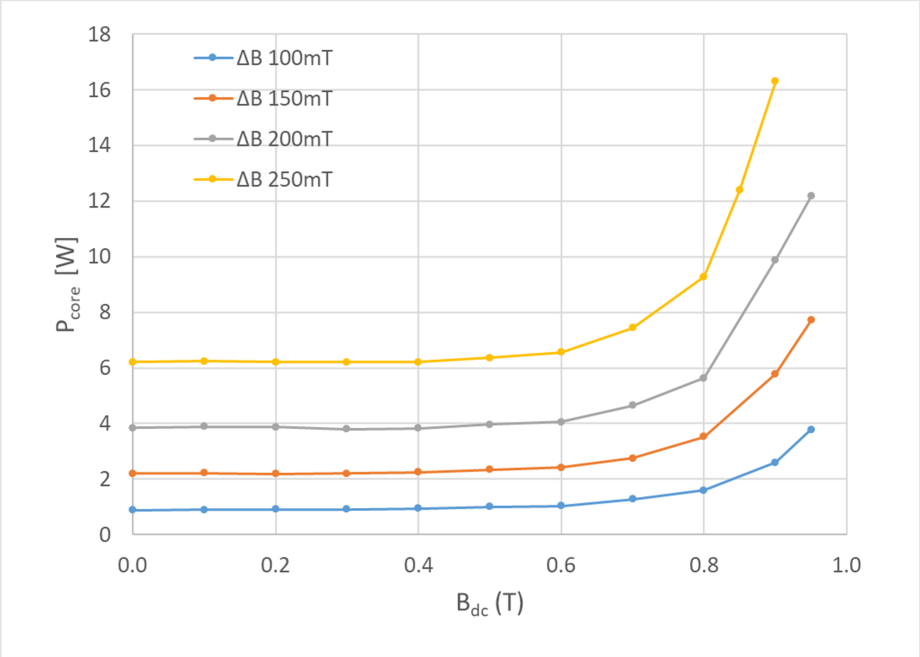

(a) Measured core loss

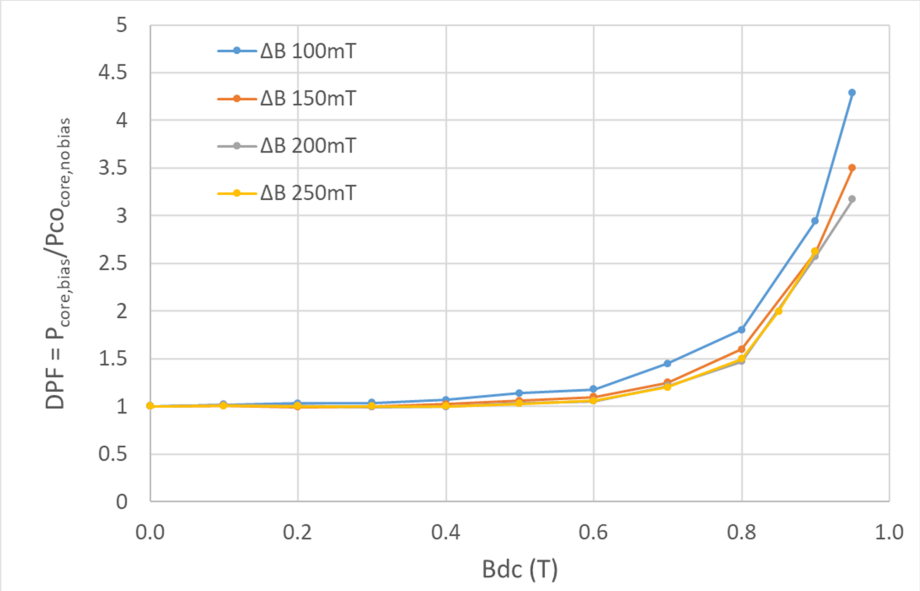

(b) DPF

Figure 4.6: Under DC bias condition for different ΔB_{pkpk}

ogy including magnetics operating with a DC flux bias, from the well-known Boost and flyback converters, to the newest solid-state transformer topologies. Experimental setups, procedures and discussion of the results are also included.

CHAPTER 5
CONCLUSION

Transformer parametric circuit and magnetic circuit have been provided for the unique designed high-frequency transformer for S4T application. Parasitic elements of the transformer with interleaved foil winding and coaxial cable winding have been identified and evaluated using analytical method, FEM model, and experimental characterization. Due to the operation cycle of S4T, there is a DC flux bias in the core. This is being offset by permanent magnets. The magnetic circuits for this design was provided. Double Pulse Test (DPT) was used to find saturation level of the transformer with and without magnets. Experimental results showed that design with permanent magnets can store much more energy than the conventional transformer. The permanent magnets can improve the saturation current level by 80%. Thought FEM model showed the 100% improvement can be achieved, researchers have identified that FEM results are not reliable and mismatch between FEM and experimental always exists. Also the position of the permanent magnets is important.[8] The distance between the magnets on the top core and on the bottom core was set to equal to the air gap, so that no virtual air gap was introduced to affect magnet performance.

AC winding loss has been studied in details. Proposed analytically methods is confirmed using FEM method and experimental tests. It was shown that the active winding could induce eddy currents in the open transformer windings resulting in AC copper loss, even though no current is present at the winding terminal. Also, it was shown that though the transition times are a much smaller part of the switching cycle, the loss during this period can be significant because the winding currents during this period vary at very high frequency. Detailed analytical methods to estimate these losses are presented. The effect of induced eddy currents in open windings in verified through FEM analysis in ANSYS

Maxwell environment. In addition, the proposed analytical method was verified using FEM analysis. Using an example transformer design, it was shown that the loss in the open (inactive) windings could be higher than the loss in the active windings and tend to increase with number of turns and frequency. In S4T, even though the AC current is relatively small ($< 30\%$ of the DC current), the eddy currents in the open windings could result in a significant AC copper loss, especially at higher frequencies.

Nanocrystalline core from MK Magnetics has been tested under no DC bias conditions and at different flux density ripple. Improved generalized Steinmetz equation utilize parameters from manufacture and provides analytical estimation of core loss. Experimental results are within 20% of analytical calculations, which shows nanocrystalline material core loss is as expected under no DC bias condition. Further, same core has been tested under DC bias conditions at different flux density ripple. And results reported unprecedented 4.3x increase in the core loss of nanocrystalline material, under non-saturated core conditions, and typical flux ripple conditions (<30%) power electronics. It is also shown that the relative core losses increase is larger at lower flux density ripple. These results have been confirmed through multiple direct and indirect measurements and for several cores of the same material from the same manufacture.

5.1 Future Work

Nanocrystalline core from MK Magnetics have been tested at different DC bias level. Unprecedented 4.3x increase in the core loss have been observed and confirmed using direct and indirect methods. However, very few studies on the nanocrystalline material core loss have been published, more testing on the nanocrystalline cores are needed to fully understand the core loss under DC bias and with permanent magnets.

The same core loss test setup and test procedure can be used to carry out further study on nanocrystalline material core loss. Recommended future studies are suggested below. First of all, different nanocrystalline material grade can be studied. So nanocrsytalline core

from Hitachi will be tested for core loss and checked whether the same DPF factor exist. Secondly, different core sizes will be studied. So different cores from same manufactures will be tested to determine whether DPF factor is related to cross section area or weight of the core. After fully understand the nanocrystalline mater core loss under DC bisa, the use of permanent magnets to offset the DC flux bias and its impact on core loss need to be studied. This will significantly help future design optimization and determine the size of the transformer. Though airgap fringing flux induced eddy current in the magnets, this loss can be reduced by moving magnets away from the air gap, which creates virtual airgap and decrease magnets performance, or by using segmented permanent magnets [25], which width are small than skin depth of N42 magnets (5mm). Finally, the permanent magnets effect on core loss and its eddy current loss needs future study.

REFERENCES

[1] R. D. Doncker, D. Divan, and M. Kheraluwala, "A three-phase soft-switched high power density dc/dc converter for high power applications," *Conference Record of the 1988 IEEE Industry Applications Society Annual Meeting*,

[2] H. Chen and D. Divan, "High-frequency transformer design for the soft-switching solid state transformer (s4t)," *2017 IEEE Applied Power Electronics Conference and Exposition (APEC)*, 2017.

[3] C. Bruce, "High frequency conductor losses in switchmode magnetic," *High Frequency Power Conversion Conference proceedings*, pp. 155–176, 1986.

[4] J Muhlethaler, J Biela, J. W. Kolar, and A Ecklebe, "Core losses under dc bias condition based on steinmetz parameters," *The 2010 International Power Electronics Conference - ECCE ASIA -*, 2010.

[5] K. Venkatachalam, C. Sullivan, T. Abdallah, and H. Tacca, "Accurate prediction of ferrite core loss with nonsinusoidal waveforms using only steinmetz parameters," *2002 IEEE Workshop on Computers in Power Electronics, 2002. Proceedings.*,

[6] M. Rauls, D. Novotny, and D. Divan, "Design considerations for high-frequency coaxial winding power transformers," *IEEE Transactions on Industry Applications*, vol. 29, no. 2, pp. 375–381, 1993.

[7] J. T. Ludwig, "Inductors biased with permanent magnets: Part i -theory and analysis," *Transactions of the American Institute of Electrical Engineers, Part I: Communication and Electronics*, vol. 79, no. 3, 273âĂŞ278, 1960.

[8] A. R. Aguilar and S. Munk-Nielsen, "Method for introducing bias magnetization in ungaped cores: "the saturation-gap"," *2014 IEEE Applied Power Electronics Conference and Exposition - APEC 2014*, 2014.

[9] J. Lu and F. Dawson, "Characterizations of high frequency planar transformer with a novel comb-shaped shield," *IEEE Transactions on Magnetics*, vol. 47, no. 10, pp. 4493–4496, 2011.

[10] G. M. Shane and S. D. Sudhoff, "Permanent magnet inductor design," *2011 IEEE Electric Ship Technologies Symposium*, 2011.

[11] X. Han, R. P. Kandula, K. Kandasamy, D. Divan, and M. Saeedifard, "Soft-switching characterization of 3.3 kv reverse-blocking sic devices," *2018 IEEE 6th Workshop on Wide Bandgap Power Devices and Applications (WiPDA)*, 2018.

[12] M. Mu, F. Zheng, Q. Li, and F. C. Lee, "Finite element analysis of inductor core loss under dc bias conditions," *IEEE Transactions on Power Electronics*, vol. 28, no. 9, 4414âĂŞ4421, 2013.

[13] P. Dowell, "Effects of eddy currents in transformer windings," *Proceedings of the Institution of Electrical Engineers*, vol. 113, no. 8, p. 1387, 1966.

[14] X. Nan and C. Sullivan, "An improved calculation of proximity-effect loss in high-frequency windings of round conductors," *IEEE 34th Annual Conference on Power Electronics Specialist, 2003. PESC 03.*,

[15] B. Carsten, "High frequency conductor losses in switchmode magnetics.," vol. 12, pp. 34–40, 43, Nov. 1986.

[16] C. Sullivan, "Computationally efficient winding loss calculation with multiple windings, arbitrary waveforms, and two-dimensional or three-dimensional field geometry," *IEEE Transactions on Power Electronics*, vol. 16, no. 1, pp. 142–150, 2001.

[17] H. Chen and D. Divan, "Soft-switching solid state transformer (s4t)," *2016 IEEE Energy Conversion Congress and Exposition (ECCE)*, 2016.

[18] W. Shen, F. Wang, D. Boroyevich, and C. W. T. Iv, "High-density nanocrystalline core transformer for high-power high-frequency resonant converter," *IEEE Transactions on Industry Applications*, vol. 44, no. 1, 213âĂŞ222, 2008.

[19] H. Kosai, Z. Turgut, and J. Scofield, "Experimental investigation of dc-bias related core losses in a boost inductor," *IEEE Transactions on Magnetics*, vol. 49, no. 7, pp. 4168–4171, 2013.

[20] A. Brockmeyer, "Experimental evaluation of the influence of dc-premagnetization on the properties of power electronic ferrites," *Proceedings of Applied Power Electronics Conference. APEC 96*,

[21] Hitachi, "Metglas amcc series cut core / finemet f3cc series cut core,"

[22] W. Shen, F. Wang, D. Boroyevich, and C. W. Tipton, "Loss characterization and calculation of nanocrystalline cores for high-frequency magnetics applications," *APEC 07 - Twenty-Second Annual IEEE Applied Power Electronics Conference and Exposition*, 2007.

[23] K. Venkatachalam, C. Sullivan, T. Abdallah, and H. Tacca, "Accurate prediction of ferrite core loss with nonsinusoidal waveforms using only steinmetz parameters," *2002 IEEE Workshop on Computers in Power Electronics, 2002. Proceedings.*,

[24] M. Magnetics, *Tape Wound Core Specialists*.

[25] K. Yamazaki and Y. Fukushima, "Effect of eddy-current loss reduction by magnet segmentation in synchronous motors with concentrated windings," *2009 International Conference on Electrical Machines and Systems*, 2009.